Title

Adipocytes reprogram cancer cell metabolism by diverting glucose towards glycerol-3-phosphate thereby promoting metastasis

Journal

Nature Metabolism, 5(9)

ISSN

2522-5812

Authors

Mukherjee, Abir

Bezwada, Divya

Greco, Francesco

et al.

Publication Date

2023-09-01

DOI

10.1038/s42255-023-00879-8

nature metabolism

Article

https://doi.org/10.1038/s42255-023-00879-8

Adipocytes reprogram cancer cell metabolism by diverting glucose towards glycerol-3-phosphate thereby promoting metastasis

Received: 5 October 2021

Accepted: 27 July 2023

Published online: 31 August 2023

Check for updates

Abir Mukherjee[1], Divya Bezwada[2], Francesco Greco[3,4], Malu Zandbergen[1], Tong Shen[5], Chun-Yi Chiang[1], Medine Tasdemir[1], Johannes Fahrmann[6], Dmitry Grapov[5], Michael R. La Frano[5], Hieu S. Vu[2], Brandon Faubert[7], John W. Newman[5], Liam A. McDonnell[4], Luigi Nezi[8], Oliver Fiehn[5], Ralph J. DeBerardinis[2,9] & Ernst Lengyel[1]

In the tumor microenvironment, adipocytes function as an alternate fuel source for cancer cells. However, whether adipocytes influence macromolecular biosynthesis in cancer cells is unknown. Here we systematically characterized the bidirectional interaction between primary human adipocytes and ovarian cancer (OvCa) cells using multi-platform metabolomics, imaging mass spectrometry, isotope tracing and gene expression analysis. We report that, in OvCa cells co-cultured with adipocytes and in metastatic tumors, a part of the glucose from glycolysis is utilized for the biosynthesis of glycerol-3-phosphate (G3P). Normoxic HIF1α protein regulates the altered flow of glucose-derived carbons in cancer cells, resulting in increased glycerophospholipids and triacylglycerol synthesis. The knockdown of HIF1α or G3P acyltransferase 3 (a regulatory enzyme of glycerophospholipid synthesis) reduced metastasis in xenograft models of OvCa. In summary, we show that, in an adipose-rich tumor microenvironment, cancer cells generate G3P as a precursor for critical membrane and signaling components, thereby promoting metastasis. Targeting biosynthetic processes specific to adipose-rich tumor microenvironments might be an effective strategy against metastasis.

Several intra-abdominally metastasizing cancers (such as gastric, colorectal and ovarian) have the propensity to metastasize to adipose tissues in the abdominal cavity, including the omentum, the small bowel mesentery and the fat appendages on the large bowel (appendices epiploicae)[1,2]. The primary metastatic site for these cancers and the site for the largest tumor is the omentum, a large fat pad in the abdominal cavity overlying the small bowel. Colonization of the omental tissue marks an essential step in the metastatic cascade of ovarian cancer

[1]Department of Obstetrics and Gynecology/Section of Gynecologic Oncology—Center for Integrative Sciences, University of Chicago, Chicago, IL, USA. [2]Children's Medical Center Research Institute, University of Texas Southwestern Medical Center, Dallas, TX, USA. [3]Fondazione Pisana per la Scienza ONLUS, San Giuliano Terme, Italy. [4]Institute of Life Sciences, Sant'Anna School of Advanced Studies, Pisa, Italy. [5]NIH West Coast Metabolomics Center, University of California, Davis, CA, USA. [6]Department of Clinical Cancer Prevention, The University of Texas MD Anderson Cancer Center, Houston, TX, USA. [7]Department of Medicine/Section of Hematology and Oncology, University of Chicago, Chicago, IL, USA. [8]Department of Experimental Oncology, IRCCS European Institute of Oncology, Milano, Italy. [9]9Howard Hughes Medical Institute, University of Texas Southwestern Medical Center, Dallas, TX, USA. e-mail: elengyel@uchicago.edu

(OvCa)[3]. The omentum, where adipocytes are the primary stromal cells, is distinct from the microenvironment of the ovary or fallopian tube where the OvCa originate. Therefore, cancer cells must rewire their metabolism to survive and proliferate in this lipid-rich environment.

We have shown that, in epithelial OvCa, omental adipocytes contribute to the selective tropism of cancer cells by the secretion of adipokines[4]. Upon interaction with the omental adipocytes, the OvCa cells transform them into 'cancer-associated adipocytes'[1], co-opting them for growth. To meet the energetic demands, OvCa cells promote lipolysis in adipocytes and take up lipids through the fatty acid receptor CD36, subsequently oxidizing these intracellular lipids[5,6]. However, it is unclear if the interaction of adipocytes with cancer cells results in additional metabolic changes in adipocytes and cancer cells. Given that increased biosynthesis of cellular components is an essential feature of proliferating cancer cells[7], the influence of adipocytes on such processes in cancer cells is yet to be determined. Moreover, no systematic metabolic analysis of the bidirectional interactions between primary human adipocytes and cancer cells has been performed.

Glucose, the primary carbon source in most tumor microenvironments (TMEs), contributes to de novo lipogenesis via citrate. However, in lipid-rich TME cancer cells use fatty acid oxidation for energy production, but any contribution of glucose-derived carbons towards lipids or phospholipid synthesis is less explored. In this Article, using untargeted global metabolomics and [^{13}C]-glucose stable isotope tracing, we show that adipocytes redirect glucose utilization in cancer cells towards glycerol-3-phosphate (G3P) synthesis. As a consequence of this rewired glucose metabolism, adipocyte-influenced cancer cells accumulate glycerophospholipids (GPLs) and triacylglycerols (TGs) necessary for their metastatic capacity.

Results

Multi-omics analyses of adipocyte–cancer cell interactions

We undertook an untargeted compartment-resolved multi-omics approach to systematically study the metabolic interactions between adipocytes and OvCa cells. Adipocytes from benign human omentum ($n = 7$) were isolated and co-cultured with OvCa cells (Fig. 1a). After (18 h) co-culture, medium was collected, and each cell type was separated into cell pellets. The cell pellets and culture medium were analyzed using three different metabolomics platforms to detect complex lipids, primary carbon metabolites and oxylipins (Fig. 1b). Fold changes of the significantly altered metabolites in cancer and adipocyte compartments were grouped on the basis of their biochemical and structural similarities, illustrated as network maps. Co-culture of cancer cells and adipocytes altered 134 metabolites in the cancer cells and 34 in the adipocytes ($P < 0.05$, mixed-effects analysis of variance (ANOVA); Fig. 1c and Extended Data Fig. 1a). Consistent with our previous finding that cancer cells use fatty acids from adipocytes for energy generation[4], we found increased TG accumulation in cancer cells ($n = 33$) (Fig. 1c) and decreased levels of fatty acids of various lengths in adipocytes ($n = 11$) (Extended Data Fig. 1a). Adipocytes also showed changes in pyruvate-derived metabolites (lactate and alanine) and tricarboxylic acid (TCA) cycle intermediates (succinate and fumarate) (Extended Data Fig. 1a) after co-culture with OvCa cells. A review of all metabolites in the co-cultured adipocytes suggests increased glucose oxidation via glycolysis and the TCA cycle. The most striking change in the cancer cells upon co-culture was an increase in GPLs ($n = 76$), with phosphatidylcholines (PCs) being the most altered metabolite, followed by phosphatidylethanolamines (PEs) (Fig. 1c). Of note, the adipocyte-induced changes in the cancer cell lipidome are distinct from those by other stromal cells (fibroblasts and pre-adipocytes) (Extended Data Fig. 1b and Supplementary Table 1).

GPLs are essential cell membrane components that are synthesized by incorporating fatty acids onto a glycerol backbone, with PC being the most abundant phospholipid[8,9]. However, GPLs can also enter the cell from the extracellular media/TME[9]. Our secretome analysis revealed that the co-culture of adipocytes with OvCa cells altered metabolite levels in the medium. Cancer cells cultured with adipocytes contributed more metabolites ($n = 83$) than adipocytes alone ($n = 15$; $P < 0.05$; Extended Data Fig. 1c). Specifically, we observed increased monoacylglycerides, cyclooxygenase-derived metabolic products and ceramides in the medium from co-cultures (Extended Data Fig. 1d). While some PCs detected in the medium were adipocyte derived, not all were taken up by cancer cells upon co-culture (Extended Data Fig. 1e). PC (34:1), one of the most abundant PCs in cancer cells[10], is released in the medium by adipocytes; however, its amount remained unchanged when co-cultured with cancer cells (Extended Data Fig. 1e), suggesting that some PCs are synthesized within cancer cells. One of the primary pathways for PC synthesis is the fatty acid acylation of G3P, which is often generated from glucose[11].

Next, we explored the relationship between gene and metabolic networks of co-cultured adipocytes and cancer cells. There were 255 and 1,065 differentially expressed genes in the adipocyte and cancer compartments, respectively (false discovery rate, FDR <0.05; Extended Data Fig. 2a,b and Supplementary Table 2). Gene set enrichment analysis revealed that co-culture leads to increased expression of cell cycle regulators in both cell types (Extended Data Fig. 2c,d). Subsequently, we carried out a combined gene and metabolite over-representation analysis to guide further investigations into the interactions between adipocytes and cancer cells. The in silico analysis identified central carbon metabolism as a critical pathway altered in both cellular compartments (Supplementary Table 3), with glycolytic pathway alterations in cancer cells co-cultured with adipocytes. In cancer cells, we found increased expression of genes regulating glycolysis, including hexokinase 2 (HK2), glycerol-3-phosphate acyltransferase 3 (GPAT3) the enzyme metabolizing G3P, and lactate dehydrogenase (Extended Data Fig. 2e). In adipocytes, phosphofructokinase was highly expressed with co-culture (Extended Data Fig. 2f). The in silico analyses suggested that co-culture with adipocytes may enhance glucose metabolism, as well as lipid metabolism[4–6], in cancer cells.

Glucose-derived carbons are used for the biosynthesis of G3P in metastatic OvCa

Our metabolomics data show that increased PC abundance is the major change in adipocyte co-cultured cancer cells. The integrated gene expression/metabolite analysis also suggested increased glycolytic activity in cancer cells co-cultured with adipocytes. Consequently, we explored if cancer cells use glucose to generate the glycerol backbone for phospholipids and TGs.

Consistent with our in silico analysis, adipocyte-derived conditioned medium (Adi CM) increased the extracellular acidification rate (ECAR) in two OvCa cell lines, showing significant increases in glycolytic rate (Fig. 2a and Extended Data Fig. 3a,b). We then considered the possibility that glucose-derived carbons enter the glycolytic branch pathway for G3P synthesis in omental tumors. To trace the flow of glucose-derived carbons in tumor tissue in the adipose TME, we performed stable isotope tracing analysis[12] on human omental explants obtained from three patients with advanced-stage high-grade serous OvCa. Cancer tissue adjacent to adipocytes was cultured ex vivo in medium containing [U-^{13}C]-glucose for 24 h, and the ^{13}C enrichment profiles were mapped for central carbon pathway metabolites (Fig. 2b). We found high labeling in m + 6 fructose-6-phosphate, m + 3 lactate, and low labeling in (m + 2 isotopologs) of TCA cycle intermediates. The absence of considerable labeling in the other isotopologs of the TCA cycle intermediates (Extended Data Fig. 3c) suggests that the cycling of glucose-derived carbons in the TCA cycle is less likely. The metastatic OvCa cells, therefore, have reduced glucose-derived carbons entering the TCA cycle (Fig. 2b).

However, the tumor explants had substantial labeling (range 42–61%) in G3P, the backbone for TG and GPLs (Fig. 2b). Consistent with these results, we observed elevated $m + 3$ labeling in

https://doi.org/10.1038/s42255-023-00879-8

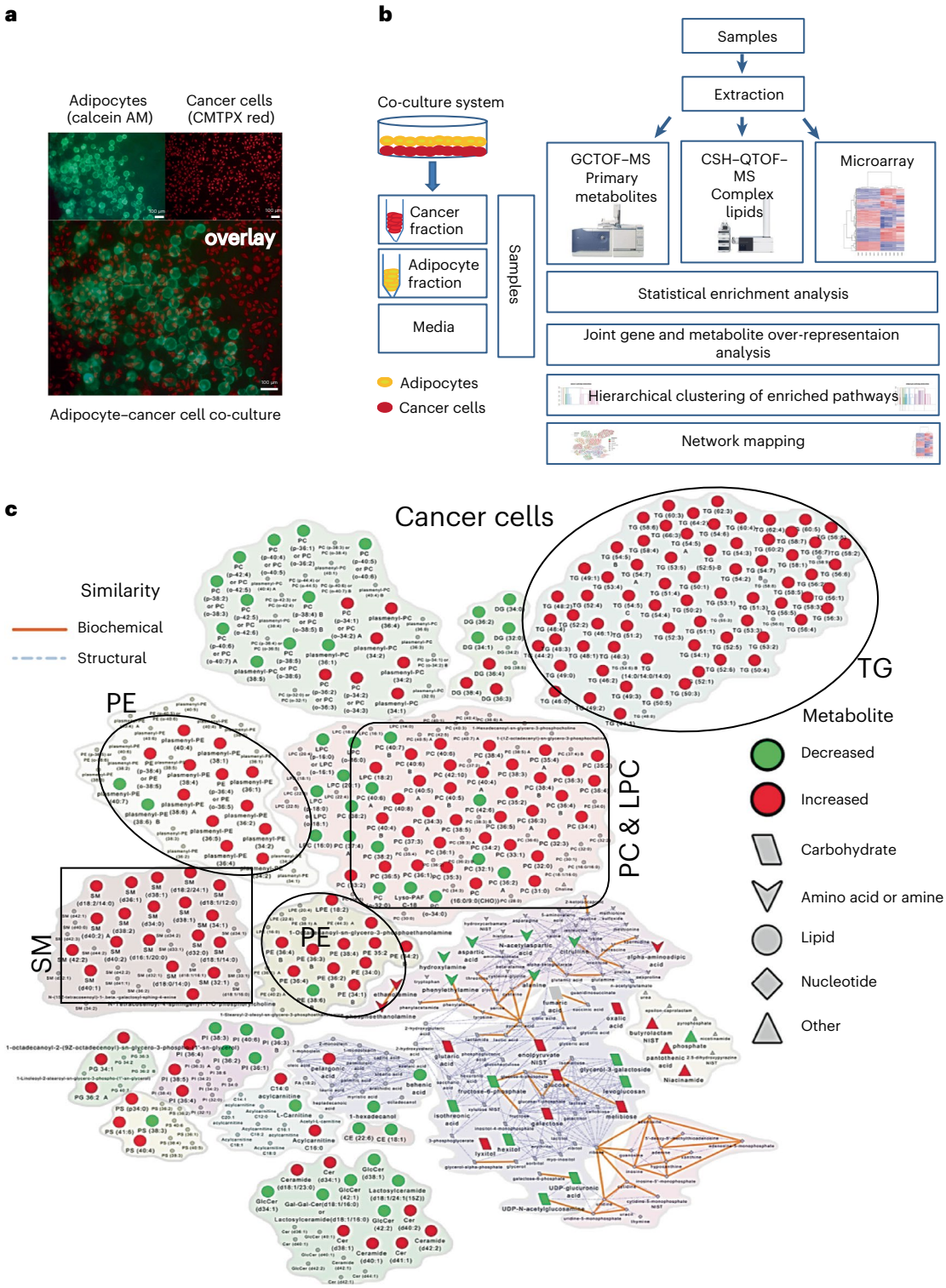

Fig. 1 | Adipocytes increase glucose metabolism and GPLs in OvCa cells. **a**, Co-culture of fluorescently (CMTPX) labeled OvCa cells (red) with calcein AM-labeled primary human omental adipocytes (green). The adipocytes float on the surface because of their lipid content ($n = 3$ independent experiments). CSH-QTOF, charged surface hybrid column-quadrupole time of flight mass spectrometer. **b**, Schematic for multi-omics analyses of co-cultured adipocytes and OvCa cells. **c**, Network map showing altered levels of metabolites (red, increase; green, decrease) in SKOV3ip1 cells with adipocyte co-culture. Biochemically and structurally similar metabolites are clustered. Orange lines connect metabolites in the same biochemical pathway, and blue lines connect structurally similar metabolites. Overall, GPLs (SM, sphingomyelin) are increased. Scale bar, 100 µm.

lysophosphocholine 18:1 (Extended Data Fig. 3d), with almost no labeling in the other isotopologs ($m + 4$ to $m + 26$) since fatty acids most likely contribute these carbons and are not derived from glucose. To determine if Adi CM increases G3P levels in cancer cells in vitro, we performed a [^{13}C]-glucose tracing experiment in cancer cells treated with Adi CM. Area-under-the-curve (AUC) analysis was performed to determine the total pool of G3P and the relative contributions of ^{13}C and ^{12}C. Adi CM treatment significantly increased total G3P levels (sum of ^{13}C

https://doi.org/10.1038/s42255-023-00879-8

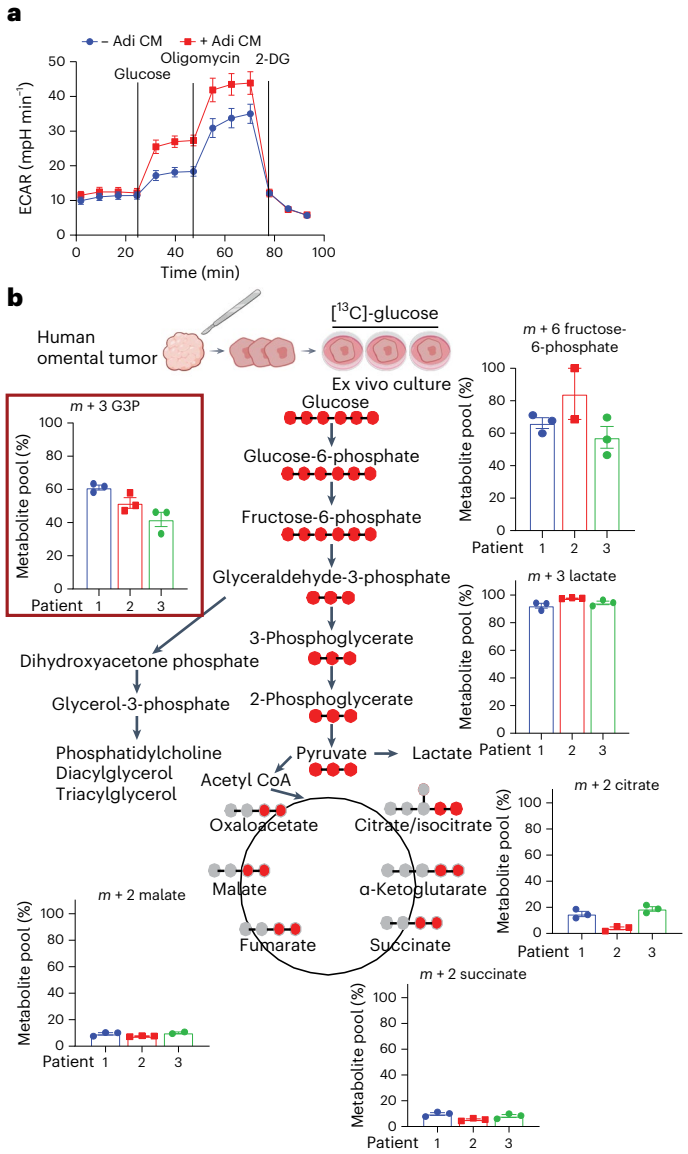

Fig. 2 | Adipocytes increase glycolysis but not oxidative phosphorylation in OvCa cells. a, SKOV3ip1 cells were treated with Adi CM for 18 h, followed by measurement of ECAR, using Seahorse XF^{e}96 analyzer ($n = 3$ independent experiments). Data represent mean ± s.e.m. **b**, [^{13}C]-glucose stable isotope tracing. Fresh omental tumor sections were incubated with [^{13}C]-glucose for 24 h, followed by MS to detect [^{13}C]-carbon enrichment of the glycolytic pathway and TCA cycle. Bar graphs depict mean ± s.e.m. ($n = 3$ independent biological samples) (adapted from BioRender.com (2023)).

and ^{12}C) in cancer cells (Extended Data Fig. 3e). We also observed a trend towards the increased contribution of ^{13}C to G3P pools in cancer cells treated with Adi CM. Compared with control media, Adi CM treatment does increase the total pool of G3P.

Overall, these findings indicate that in cancer tissue adjacent to adipocytes, glucose is partially utilized for the biosynthesis of the G3P. While the flow of glucose-derived carbons into the pentose phosphate pathway and nucleotide synthesis has been explored[13], little is known about the rewiring of glucose for the synthesis of G3P in the context of metastasis.

GPAT3 regulates adipocyte-induced GPL synthesis

Next, we explored how glucose-derived G3P is metabolized by OvCa cells when adipocytes are present. Adipocyte co-culture increased GPAT3 messenger RNA expression in cancer cells (Extended Data Fig. 2e). GPAT3 is an enzyme upstream of GPL and TG synthesis that converts G3P into lysophosphatidic acid[11] (Fig. 3a). Consistent with GPAT3 regulation by adipocyte–cancer cell co-culture in vitro, we found GPAT3 protein expression in human omental metastasis from high-grade serous OvCa. Higher GPAT3 expression was detected in OvCa cells (Fig. 3b), and much lower expression in stroma and adipocytes. Using liquid chromatography (LC)–mass spectrometry (MS) to perform lipidomics, GPAT3 knockdown in OvCa cells co-cultured with adipocytes resulted in reduced GPLs and TGs, suggesting that adipocytes promote GPAT3-dependent GPL synthesis (Fig. 3c). The loss of GPAT3 reduced omental metastatic tumor burden in vivo (Fig. 3d and Extended Data Fig. 4), indicating that GPL synthesis in cancer cells is required for efficient omental metastasis.

Adipocyte-induced HIF1α directs glucose-derived carbons to GPL synthesis

Since glucose-derived carbons are used for G3P synthesis, we next sought to understand how adipocytes regulate the altered use of glucose in OvCa cells. Increased ECAR (Fig. 2a) is an energetic profile frequently associated with the hypoxia-inducible factor (HIF) 1α expression[14,15]. We considered that adipocytes possibly reprogram OvCa cell metabolism through HIF1α[16]. Adipocyte co-culture increased HIF1α protein expression in multiple OvCa cell lines under normoxic conditions (Fig. 4a and Extended Data Fig. 5a). HIF1α, in the presence of oxygen, undergoes prolyl hydroxylation and proteasomal degradation, explaining why HIF1α protein is low under normoxic conditions. To determine whether adipocytes help stabilize HIF1α protein, we used a surrogate luciferase reporter plasmid, where the luciferase expression/activity is regulated by the oxygen-dependent degradation domain (ODD) of HIF1α (refs. 17,18). The stable transfection of the ODD-luciferase plasmid, followed by Adi CM treatment, increased luciferase activity, suggesting that adipocytes stabilize HIF1α (Fig. 4b).

To identify the downstream targets of adipocyte-induced HIF1α in cancer cells, we performed an MS-based proteomic analysis[19]. Proteomic analysis showed that HIF1α knockdown (Extended Data Fig. 5b) altered the adipocyte-induced proteome of OvCa cells, reducing 82 and increasing 22 proteins (Extended Data Fig. 5c and Supplementary Table 4). HIF1α knockdown reduced protein expression of HK2 and the lactate/pyruvate transporter SLC16A3 (also known as MCT4) (Fig. 4c). Consistent with the proteomic data, adipocyte co-culture induced HK2 mRNA and protein levels in OvCa cells, dependent on HIF1α expression (Fig. 4d). We also found increased HIF1α and HK2 expression in the epithelial tumor compartment adjacent to adipocytes in patients with omental metastasis (Fig. 4e). Adipocyte-induced HIF1α also increased G3P dehydrogenase (GPD1) (Extended Data Fig. 5d), an enzyme that converts the glycolytic intermediate dihydroxyacetone phosphate to G3P (Fig. 3a). Therefore adipocyte-induced HIF1α regulates the flow of glucose into G3P.

HIF1α knockdown inhibited the effect of adipocytes on glycolysis (ECAR; Extended Data Fig. 5e,f). Consistent with the energetic profile, HIF1α knockdown reduced glycolytic intermediates (Fig. 4f) and increased TCA cycle metabolites (Fig. 4g) with adipocyte co-culture. This suggests that adipocytes induce 'pseudo-hypoxia'[20]. HIF1α knockdown blocked a majority of adipocyte-induced triacylglycerol (24/28), PEs (19/30) and ether-linked PCs (5/6), as well as other membrane lipids such as sphingomyelins (7/13) and ceramides (8/14) (Extended Data Fig. 6 and Supplementary Table 5). So, the adipocyte-induced HIF1α-driven transcriptional program regulates glucose utilization towards GPL and TG synthesis in cancer cells.

Since adipocyte co-culture and Adi CM regulates glucose metabolism in cancer cells in an HIF1α-dependent manner, we sought to identify adipocyte-secreted soluble factors that regulate HIF1α expression in cancer cells. Fractionation of adipocyte CM using a size-exclusion

https://doi.org/10.1038/s42255-023-00879-8

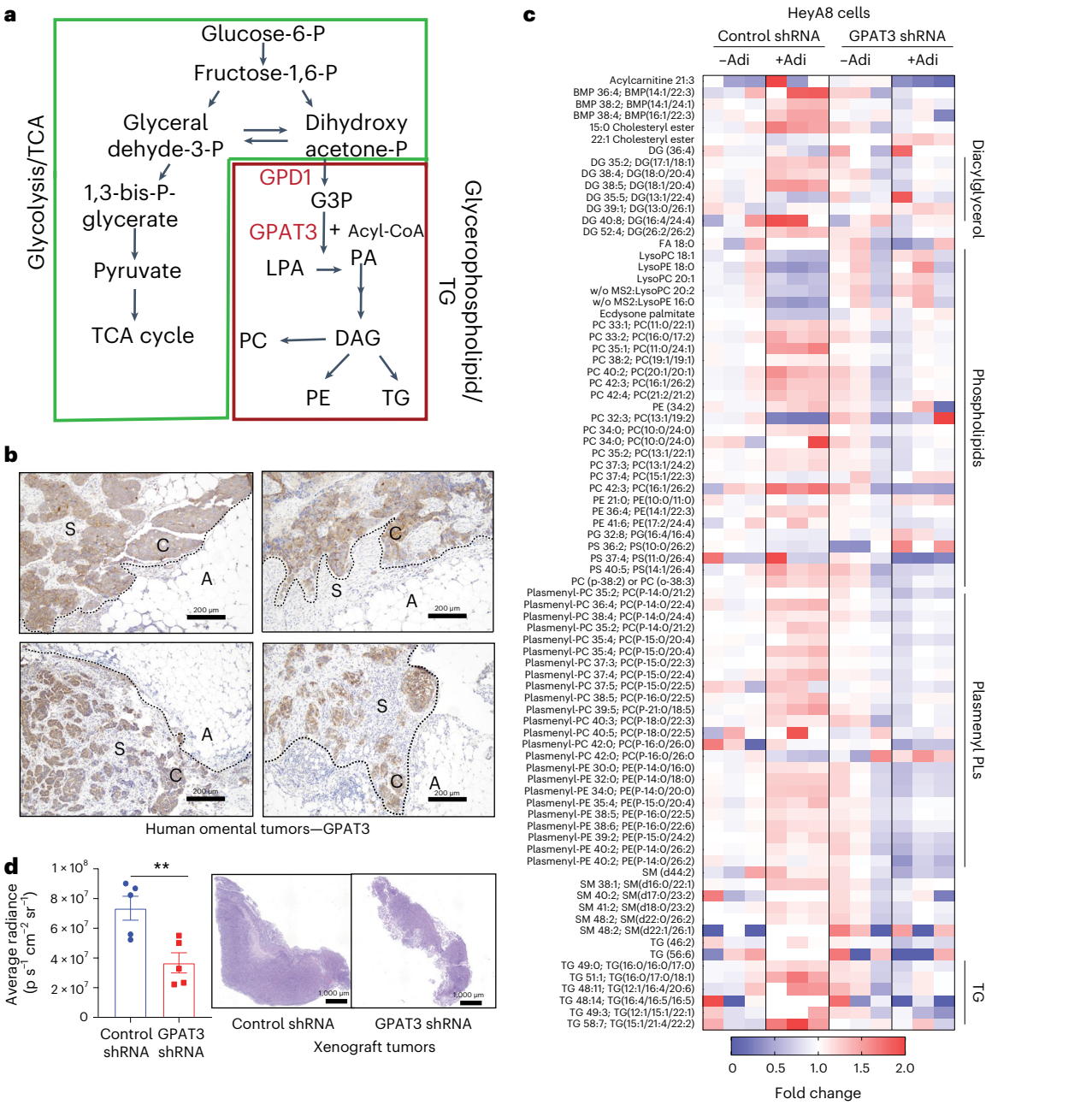

Fig. 3 | GPAT3 regulates GPL synthesis. a, Schematic. GPAT3 catalyzes the initial step in de novo GPL and TG synthesis. **b**, GPAT3 expression in serial sections of patients with high-grade serous OvCa metastatic omental tumor. GPAT3 expression is more abundant in the epithelial tumor compartment. A, adipocytes; C, cancer; S, stroma. Dotted lines depict invasive front. $n = 4$ independent biological samples. **c**, Lipidomics on control and GPAT3 shRNA OvCa cells co-cultured with omental adipocytes for 18 h. The heat map shows fold change of significantly altered lipid species (two-tailed t-test, $P < 0.05$). Lipid species: DG, diacylglycerol; SM, sphingomyelin; BMP, bis(monoacylglycerol) phosphate. **d**, Left: HeyA8-luciferase OvCa cells with stable control or GPAT3 knockdown were injected intraperitoneally into nude mice ($n = 5$) and subsequently imaged using IVIS spectrum in vivo imaging system. Luciferase signal was quantitated to determine tumor burden (two-tailed t-test, $^{**}P = 0.0081$, mean ± s.e.m.). Right: H&E-stained sections of entire omental tumors.

filter revealed that the HIF1α inducing activity is present in the non-metabolite fraction of adipocyte CM (Extended Data Fig. 5g). We and others have demonstrated that omental adipocytes secrete several cytokines/adipokines[21] that promote metastasis to the omentum[4]. Treatment of OvCa cells with IL-6, IL-8 and MCP-1 increased HIF1α expression under normoxic conditions, with the most substantial effect from IL-6 (Extended Data Fig. 5h). Neutralizing antibodies against IL-6 and MCP-1 abrogated adipocyte-induced HIF1α induction, while blocking IL-8 had minimal effect (Extended Data Fig. 5i). Blocking downstream IL-6 signaling, using either STAT3 or JAK kinase inhibitors, led to a reduction in adipocyte CM-induced HIF1α, while a MEK inhibitor did not affect adipocyte-induced HIF1α expression (Extended Data Fig. 5j). In summary, adipocytes induce HIF1α in cancer cells through an IL-6, JAK/STAT-driven signaling pathway.

Reduction of HIF1α expression inhibits omental metastasis

We used a xenograft mouse model to determine the impact of dysregulated HIF1α on OvCa metastasis and understand the flow of

https://doi.org/10.1038/s42255-023-00879-8

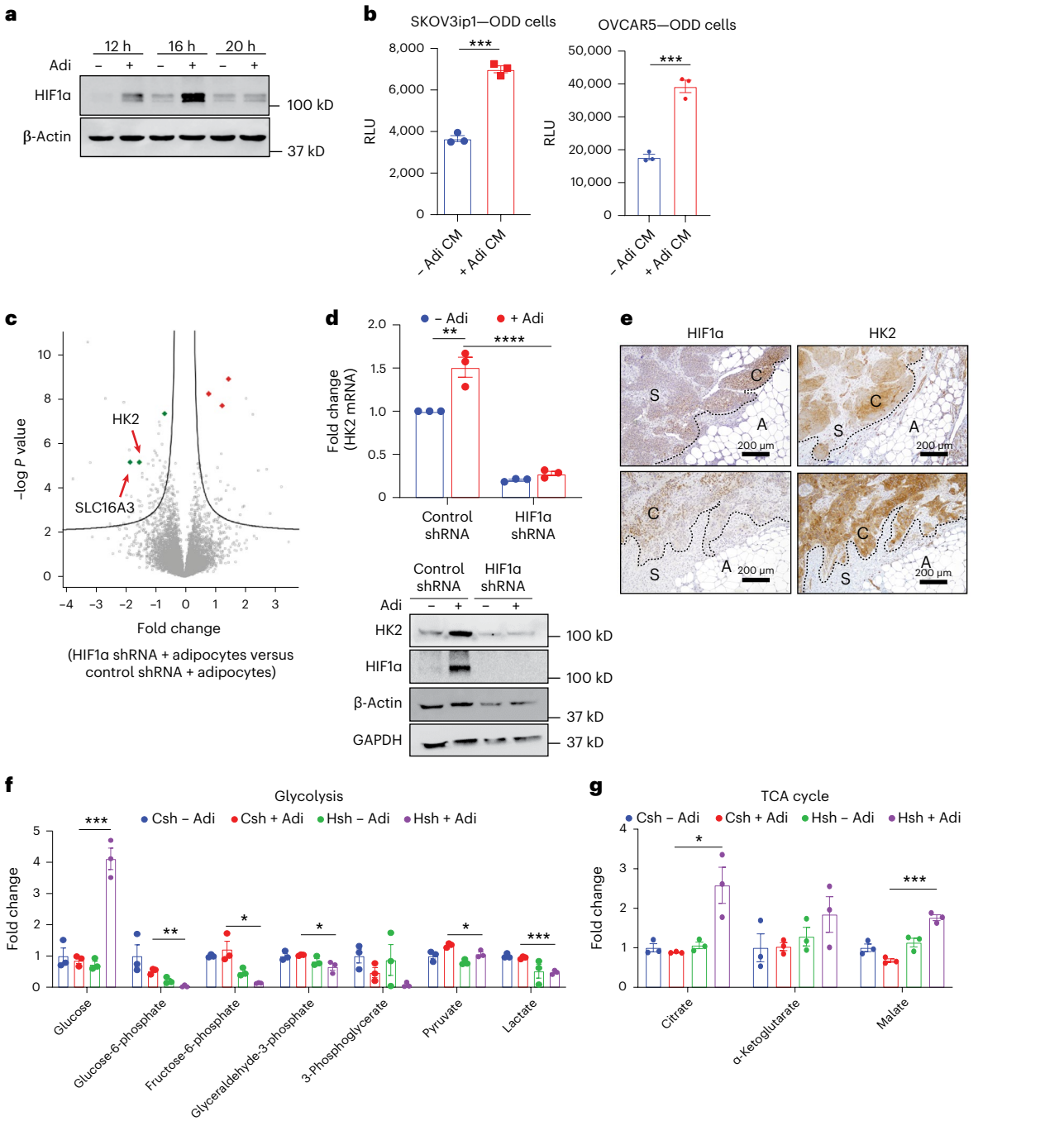

Fig. 4 | Adipocyte-mediated HIF1α expression regulates glucose utilization in cancer cells. a, Immunoblot of HIF1α in SKOV3ip1 cells co-cultured with primary human adipocytes (Adi) for the indicated times. **b**, SKOV3ip1 and OVCAR5 stably expressing the ODD of HIF1α were treated with Adi CM for 6 h, and luciferase activity was determined using a luminometer (***$P < 0.001$, two-tailed t-test, $n = 3$ independent experiments). Bar graphs depicts mean ± s.e.m. RLU, relative luminescence units. **c**, MS of proteins extracted from OvCa cells stably transfected with shHIF1α and cultured ± adipocytes. Volcano plot showing proteins regulated by adipocyte-induced HIF1α expression analyzed using a two-sided t-test with an FDR of 0.05 and an S_0 value of 0.1. **d**, qPCR (top) and immunoblot (bottom) of HIF1α and HK2 in SKOV3ip1 HIF1α knockdown cells after adipocyte co-culture for 16 h ($n = 3$ independent experiments). Bar graphs depicts mean ± s.e.m., two-way ANOVA **$P = 0.0019$, ***$P < 0.0001$). **e**, Immunohistochemistry for HIF1α and HK2 using serial sections of human omental tumors from patients with high-grade serous OvCa. A, adipocytes; C, cancer; S, stroma. Dotted lines depict invasive front. $n = 4$ independent biological samples, 2 shown. **f**,**g**, Metabolomics. Control and HIF1α knockdown SKOV3ip1 cells co-cultured with adipocytes for 18 h (two-tailed t-test, *$P < 0.05$, **$P = 0.0012$, ***$P < 0.0005$). Bar graphs show fold changes (compared with control shRNA Adi) in metabolites of the glycolytic pathway (**f**) and the TCA cycle (**g**). Csh, control shRNA; Hsh, HIF1α shRNA. $n = 3$ independent experiments. Bar graphs depicts mean ± s.e.m. (two-tailed t-test, *$P = 0.02$, ***$P = 0.0002$).

glucose-derived carbon in these tumors. Mice injected intraperitoneally with stable HIF1α knockdown OvCa cells had much smaller omental metastases (Fig. 5a). The HIF1α knockdown tumors had no change in apoptosis levels, nor were there any differences in proliferation (Fig. 5b). Ex vivo co-culture of HIF1α knockdown cells with human omental tissue did not affect the ability of OvCa cells to adhere or proliferate (Extended Data Fig. 7a,b) suggesting that HIF1α knockdown also do not affect the initial steps of omental colonization[22].

Previously we showed that adipocyte co-culture increased lipid peroxidation in OvCa cells[5,6]. Using 4-hydroxynonenal (4-HNE) adducts as a read-out for lipid peroxidation, we found increased staining intensities in HIF1α knockdown tumors (Fig. 5b). Consistent with the in vivo data, HIF1α knockdown cells cancer cells co-cultured with adipocytes showed significantly higher amount of malondialdehyde (MDA), a marker of lipid (polyunsaturated fatty acid) peroxidation (Fig. 5c). Both in vivo and in vitro data show that blocking HIF1α expression in cancer cells in the presence of adipocytes increased lipid peroxidation in cancer cells. Since uncontrolled lipid peroxidation causes ferroptosis[23], we next explored if the knockdown of HIF1α sensitized OvCa cells towards ferroptosis-mediated cell death. While we observed increased lipid reactive oxygen species (ROS) levels in control short hairpin RNA (shRNA) cells with Adi CM, the knockdown of HIF1α exacerbated the levels (Fig. 5d and Extended Data Fig. 7c). GPX4 is the primary enzyme responsible for removing membrane lipid peroxides[24]; so, we measured the survival capacity of OvCa treated with RSL3 (a GPX4 inhibitor)[25]. In the presence of Adi CM, HIF1α knockdown cells were sensitive to the inhibition of GPX4 (Fig. 5e). Further, reversal of cell viability by ferrostatin (a ferroptosis inhibitor[25]) but not by zVAD-FMK (a pan-caspase inhibitor) showed that HIF1α knockdown cells undergo ferroptosis, an apoptosis-independent cell death (Fig. 5e).

Given that GPAT3 knockdown reduced adipocyte-induced GPLs abundances in cancer cells (Fig. 3c), we explored if GPAT3 knockdown also affects lipid peroxidation and sensitivity of cancer cells to ferroptosis. GPAT3 knockdown had no effect on adipocyte-induced lipid-ROS levels (Extended Data Fig. 7d,e) in vitro, nor were any differences observed in the formation of the 4-HNE adducts in xenograft omental tumors (Extended Data Fig. 7f). Unlike HIF1α, GPAT3 knockdown did not increase the sensitivity of Adi CM treated cells towards RSL3 (Extended Data Fig. 7g). GPAT3 inhibition does not increase lipid ROS or sensitize cancer cells to ferroptosis.

To evaluate the effect of HIF1α knockdown on glucose utilization in vivo, tumor-bearing mice (control/scrambled or HIF1α shRNA) were infused with [U-^{13}C]-glucose[26]. Upon necropsy, omental tumors were excised, and carbon distribution was measured using MS (Fig. 5f). HIF1α knockdown reduced the flow of glucose into glycolysis (lactate $m+3$ and 3-phosphoglycerate $m+3$) and significantly reduced $m+3$ labeling of G3P (Fig. 5g). These data provide evidence for the diversion of glucose towards G3P synthesis by HIF1α in vivo.

Spatial distribution of GPLs in human omental metastatic tumors

To clinically validate the effect of adipocytes on GPL synthesis, we carried out imaging mass spectrometry (IMS) analysis on sections of human omental tumors. On the basis of our previous studies, we observed that the effect of adipocytes on cancer cells is dependent on their proximity to adipocytes. Therefore, to determine the adipocyte-induced phospholipid changes in cancer cells, we evaluated the differences in phospholipid species in tumor cells at the leading edge invading into adipocytes compared with cancer cells farther away (more than 200 µm from the adipocytes). Fresh frozen omental tumor sections from three patients with high-grade serous OvCa were coated with norharmane, a dual polarity matrix ideal for phospholipid analysis[27]. Subsequently, images of metabolites (ions ranging between 150 and 2,000 m/z) were taken using matrix-assisted laser desorption/ionization (MALDI) (Fig. 6a), and metabolites in cancer cells adjacent to the adipocytes were compared with cancer cells further away (Fig. 6b,c). To identify metabolites that distinguished the two groups of cancer cells, we carried out a receiver operating curve (ROC) analysis (Supplementary Table 6). The analysis showed that cancer cells adjacent to adipocytes had a higher abundance of PCs, while those at a distance had more phosphatidylinositol (PI) (Fig. 6d,e). This corroborates our observation using primary adipocytes that adipocytes adjacent to cancer cells increase PCs in tumor cells.

Discussion

The symbiotic relationship between adipocytes and cancer cells explains why omental tumors are the most common and the largest in abdominally metastasizing cancers such as ovarian and gastric[28]. Tumor cells interacting with adipocytes in the microenvironment induce lipolysis in adipocytes, and fatty acids transferred to cancer cells are used for energy production[1]. In addition, surgical removal of the omentum at early or metastatic disease reduces the recurrence risk in abdominally metastasizing tumors[29,30]. In these tumors, the interaction of omental adipocytes and cancer cells influences disease outcomes. Our systematic multi-omic analyses of the adipocyte-induced metabolic changes in cancer cells revealed that an increased glycolysis rate facilitates the use of glucose for G3P and GPL synthesis. GPLs, regulated by GPAT enzymes, are essential components of cellular lipid membranes that are important for cell division[11] and are precursors for pro-growth signaling molecules. Furthermore, GPL can be recycled in nutrient-depleted conditions (or when mTOC1 is inhibited) to generate TG to meet the energetic cellular demands via fatty acid oxidation[31]. Therefore, GPL abundance is essentially linked to cancer cell proliferation. Not surprisingly, increased GPL levels (PCs and PEs) are observed in bladder, kidney and colorectal cancers[32,33].

We found that adipocyte co-culture stabilizes HIF1α expression in OvCa cells, leading to increases in the glycolytic rate and the flow of glucose-derived carbons towards G3P and GPL synthesis, thereby supporting metastatic colonization (Fig. 6f). It is well known that glucose-derived carbons branching out into the pentose phosphate, hexamine biosynthesis and glycogenesis pathways have pro-tumorigenic effects. We now show the role of another glycolytic branch pathway (G3P synthesis) in OvCa metastasis. In tumors adjacent to omental adipose tissue, glucose-derived carbons flow into G3P for the synthesis of GPL and TG, and blocking this pathway reduced metastasis in xenograft mouse models. We also show that some PCs are synthesized in cancer cells rather than transported from the extracellular space. While OvCa cells may lack the capacity to transport certain species of PCs across the cell membrane, the synthesis of PLs via G3P

Fig. 5 | Reduction of HIF1a expression inhibits omental metastasis. Xenograft intraperitoneal metastasis model. **a**, Left: SKOV3ip1 HIF1α shRNA cells were injected intraperitoneally ($n=10$ mice per group), and tumor burden is shown with shcontrol on the left and shHIF1α on the right with omental tumor outlined in yellow. Right: tumor burden was measured as omental metastatic weight. Bar graphs depicts mean ± s.e.m. (two-tailed t-test, $^{***}P<0.0008$). **b**, Cleaved caspase 3, Ki-67 and 4-HNE staining in serial sections of omental tumors generated from **a** ($n=5$ tumors per group were stained). Csh, control shRNA; Hsh, HIF1α shRNA (two-tailed t-test, $^{**}P<0.01$, mean ± s.e.m.). **c**, Lipid peroxidation: control and HIF1α knockdown cells were co-cultured with adipocytes for 18 h, and intracellular MDA levels were determined ($n=3$ independent experiments). Bar graphs depicts mean ± s.e.m. (two-way ANOVA, $^{****}P<0.0001$; NS, not significant). **d**,**e**, Control and HIF1α shRNA transduced SKOV3ip1 cells were treated with Adi CM: cells were stained using Bodipy 581/591 C11 dye and fluorescent emissions (at 520 nm) were measured every couple of hours using Incucyte to quantify lipid ROS production ($n=3$ independent experiments; data depict mean ± s.e.m.) (**d**); MTT assay carried out to determine the viability of cancer cells after treatment with the indicated small molecule compounds ($n=3$ independent experiments; two-way ANOVA, $^{****}P<0.0001$, mean ± s.e.m.) (**e**). **f**, Stable isotope tracing in tumor-bearing mice with HIF1α knockdown cancer cells. (adapted from BioRender.com (2023)). **g**, [^{13}C]-glucose derived labeling of G3P and glycolytic intermediates in omental tumors as in Fig. 2c ($n=5$ mice). Bar graphs depict mean ± s.e.m., two-way ANOVA, $^{**}P=0.0045$, $^{***}P<0.0008$, $^{****}P<0.0001$.

https://doi.org/10.1038/s42255-023-00879-8

may have the advantage of sequestering free fatty acids as neutral lipids (TG) and reducing their toxic effects[34–36]. Therefore, colonizing OvCa cells may have adapted to the lipid-rich TME with enhanced G3P biosynthesis.

The lack of patient-matched primary and metastatic tumors prevented us from comparing the relative enrichment of glucose-derived carbons in cancer cells growing in two distinct microenvironments. We could not establish if glucose-derived G3P synthesis occurs exclusively

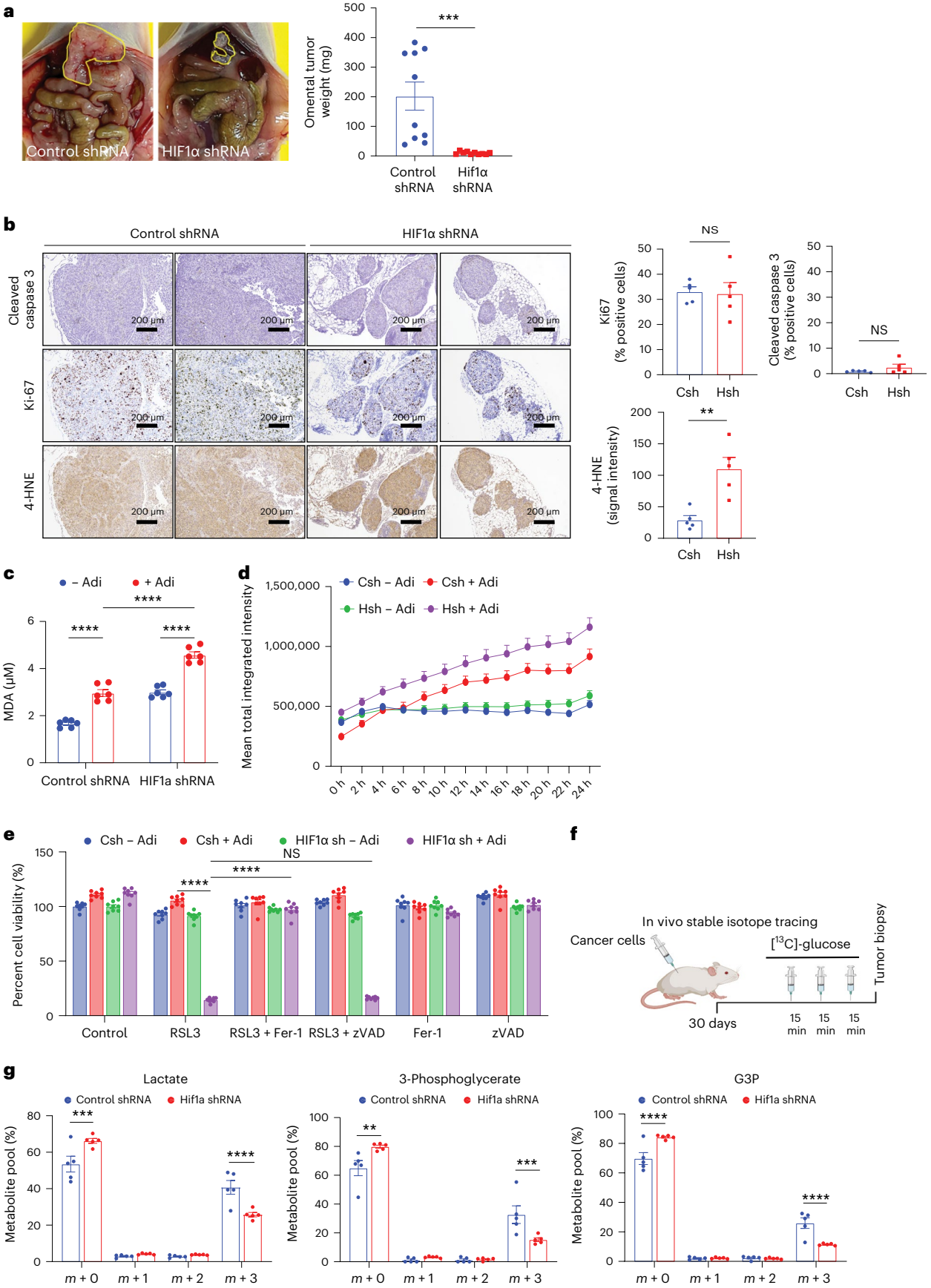

https://doi.org/10.1038/s42255-023-00879-8

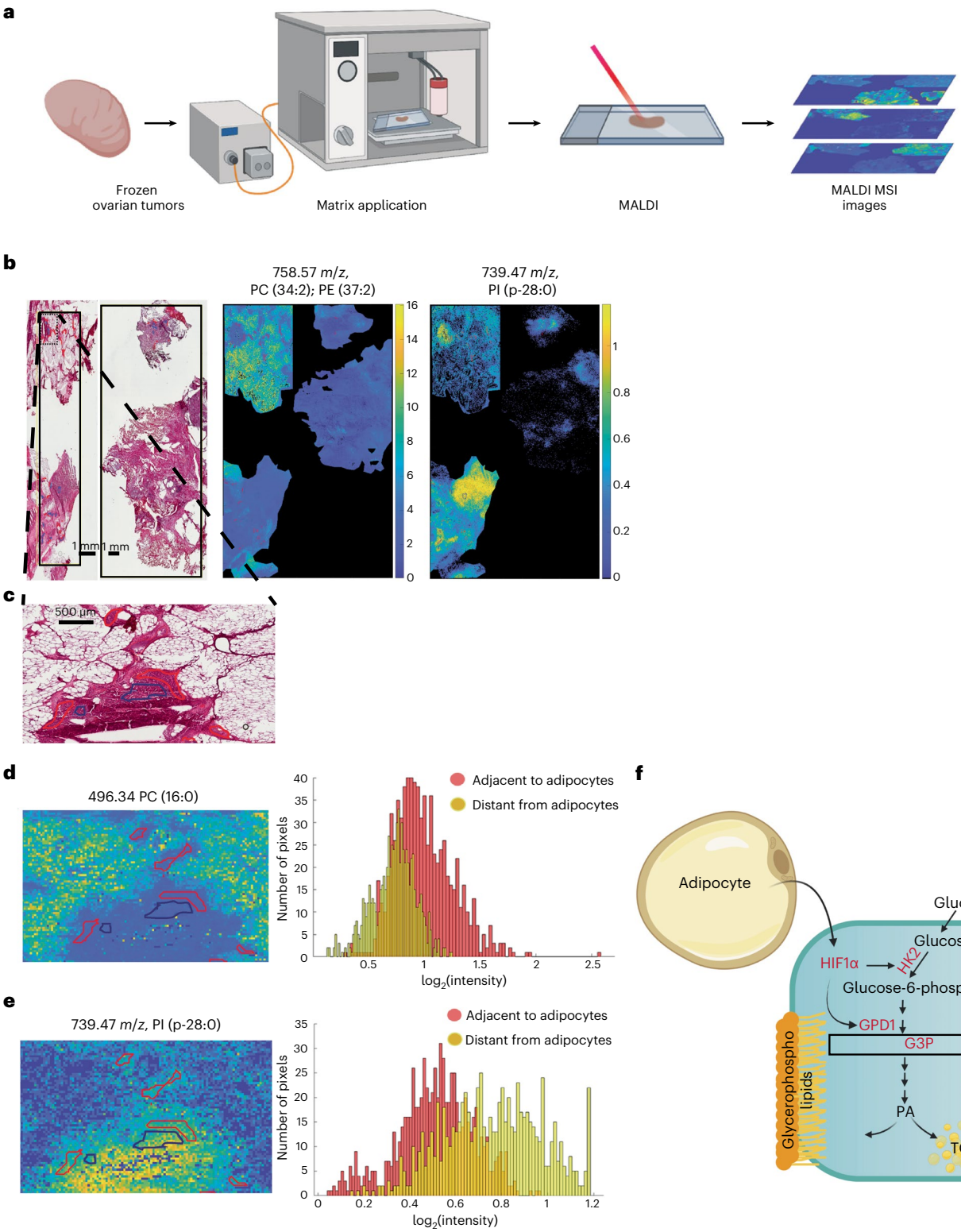

Fig. 6 | Cancer cells adjacent to adipocytes have increased PC. Spatial analysis of GPLs using IMS. **a**, Schematic for IMS analysis of ovarian high-grade serous tumor samples (adapted from BioRender.com (2023)). **b**–**e**, Histology and MALDI IMS analysis of frozen omental tumor sections ($n = 3$ independent biological samples): H&E-stained tissue with annotated tumor regions (black boxes) that were analyzed using MALDI (**b**, left) and spectral distribution of ions (496.34 *m/z* and 739.47 *m/z*) corresponding to the selected area (black boxes) on the H&E slide (**b**, right); Enlarged section of the tumor area (used for IMS analysis), showing two groups of cancer cells, adjacent (red) or distant (blue) from adipocytes (**c**); optical images using MALDI IMS of PC (16:0) (higher adjacent to adipocytes as measured by the AUC-orange) (**d**) and phosphatidylinositol (PI) p-28:0 (lower adjacent to adipocytes as measured by the AUC-orange) (**e**) corresponding to the H&E section shown in **c**, with MALDI images of ions shown on the left and the pixel intensities of the ions in the selected area on the right. **f**, Illustration of the adipocyte–OvCa cell interactions leading to altered glucose utilization in OvCa cells. Adipocytes stabilize HIF1α protein in OvCa cells. Subsequently, HIF1α transactivates HK2 and glycerol-3-phosphate dehydrogenase (GPD1). The combined activity of these two enzymes increases G3P levels in OvCa cells, forming the backbone for the synthesis of TGs and GPLs (created with BioRender.com (2023)).

in metastatic tumors. However, since (1) primary ovarian tumors originate in an environment that lacks adipocytes, (2) adipocytes increase the glycolytic rate in cancer cells and (3) the lipidomic changes in cancer cells are adipocyte specific, enhanced synthesis of G3P in cancer cells is probably a feature of adipose-rich environments.

We also show that omental adipocytes stabilize HIF1α independent of hypoxia, which diverts glucose-derived carbons to G3P, thereby generating the backbone for GPLs and TG synthesis. In our experimental approach, under adipocyte-induced 'pseudo-hypoxia', cancer cells are not reliant on glucose for fatty acid synthesis. Given the abundance of lipids in the adipocyte-rich TME, there is no need for the metastatic cancer cells to synthesize fatty acids. In adipocyte-rich TMEs, cancer cells have a distinct glucose metabolic profile. This is in contrast to hypoxic conditions, where glucose generates both G3P backbone and saturated fatty acids for PC synthesis[10].

Several mechanisms contribute to the reduced tumor burden observed in HIF1α knockdown xenografts. First, HIF1α knockdown xenografts showed a reduced flow of glucose into G3P towards TG and GPL synthesis. Secondly, in vitro adipocyte co-cultured HIF1α knockdown cells have increased lipid ROS and lipid peroxidation productions, making them uniquely susceptible to GPX4 inhibition. In addition, HIF1α knockdown xenograft tumors showed increased toxic lipid peroxidation adducts[37]. Consistent with our findings, in fibrosarcoma cells, reduced HIF1α expression increases lipid peroxidation and, subsequently ferroptosis[38]. While the knockdown of GPAT3 also reduces adipocyte-induced GPLs in cancer cells, no change was observed in the lipid peroxidation levels or the sensitivity of cancer cells towards GPX4 inhibition. Therefore, the sensitivity to ferroptosis is specific to HIF1α inhibition. While it is yet to be determined if HIFα knockdown reduces the capacity of OvCa cells to remove toxic membrane-derived lipid peroxides, we observed accumulation of polyunsaturated plasmalogens such as PE P-40:6 (known to induce ferroptosis[39]) in HIF1α knockdown cells co-cultured with adipocytes.

This study expands our current understanding of cancer-associated adipocytes by demonstrating a complex symbiotic relationship with cancer cells and a role in completely rewiring cancer cell metabolism[2]. Adipocytes support the extreme energy and biosynthetic requirements of cancer cells through a combination of adipokine secretion, lipolysis and, as we show in this study, the reprogramming of glucose metabolism.

Methods

Cell lines and reagents

SKOV3ip1, HeyA8, OVCAR5 (Gordon Mills, University of Texas MD Anderson Cancer Center, Houston) and 293T (Lucy Godley, Northwestern University, Chicago) cells were cultured as described previously[5]. TYKnu cells (Gottfried Koneczny, University of California, California) were cultured in Eagle's minimal essential medium supplemented with 10% fetal bovine serum. All cells were cultured in an incubator maintained at 37 °C with 5% CO_2. All experiments were performed using mycoplasma-negative and authenticated cell lines. Cell lines were tested every three months for mycoplasma and genotyped for authentication purposes (IDEXX Bioresearch short tandem repeat marker profiling). Neutralizing antibodies against human IL-6 (cat. no. MAB206, 100 ng ml^{-1}), IL-8 (cat. no. MAB208, 100 ng ml^{-1}), MCP-1 (cat. no. AB279, 100 µg ml^{-1}) and isotype specific control were purchased from R&D Systems. Recombinant human cytokine/chemokines IL-6 (cat. no. 200-06), MCP-1 (cat. no. 300-04) and IL-8 (cat. no. 200-08) was purchased from PeproTech and used at a concentration of 10 ng ml^{-1}. The JAK inhibitor AZD-1480 (HY-10193) and STAT3 inhibitor STATTIC (HY-13818) were purchased from MedChemExpress, and the MEK inhibitor (PD98059) was purchased from Cell Signaling Technology. 1S, 3R-RSL3 (RSL3) was purchased from Sigma-Aldrich (cat. no. SML2234) and zVAD-FMK (zVAD) from Selleckchem (cat. no. S7023). Poly-L-lysine solution 0.1%, norharmane, high-performance liquid chromatography (HPLC)-grade chloroform and LC–MS-grade methanol were purchased from Sigma-Aldrich. Histology-grade solvents and Eosin G or Y (alcoholic solution 0.5%) were purchased from DiaPath S.p.A.; Harris hematoxylin was obtained from VWR International, LLC. LC–MS-grade water was purchased from Thermo Fisher Scientific, and indium-tin oxide (ITO)-coated glass slides for MALDI mass spectrometry imaging (MSI) were obtained from Bruker Daltonics.

Isolation of primary adipocytes and cell culture

Human primary omental adipocytes, stromal vascular fraction (SVF) and normal omental fibroblasts were isolated as previously described[4,40,41]. Briefly, freshly excised omental tissues were digested using 0.2% collagenase type I enzyme for 1 h and separated from the SVF using 250 µm nylon mesh. Adipocytes were repeatedly washed with medium (Dulbecco's modified Eagle medium (DMEM)/F12 medium with 1% streptomycin and 1% penicillin) and centrifuged to remove contaminating cells. Isolated adipocytes were cultured in DMEM/F12 medium supplemented with 0.1% fatty acid-free bovine serum albumin (Roche), 100 U ml^{-1} penicillin and 100 µg ml^{-1} streptomycin. Co-culture of adipocytes with cancer cells was carried out in 1:5 packed cell adipocyte volume (PCV) to serum-free medium. The residual tissue after collagenase I digestion was further digested using collagenase III (3 mg ml^{-1}) and hyaluronidase (0.5 mg ml^{-1}) overnight, and the fibroblasts isolated were cultured in DMEM medium supplemented with 10% fetal bovine serum and minimal essential vitamins and amino acids. The cells in the SVF were grown to confluency using the fibroblast medium, to obtain pre-adipocytes. These pre-adipocytes were subsequently passaged once to generate conditioned medium.

To generate conditioned medium from adipocytes, normal omental fibroblasts and pre-adipocytes, cells were cultured in DMEM/F12 (supplemented with 0.1% fatty acid, 1% streptomycin and 1% penicillin) medium for 72 h, after which medium was removed and filtered through a 0.8 µm syringe filter. Isolated adipocytes and SKOV3ip1 cells were stained with Calcein AM (10 µM) in DMEM/F12 medium for 20 min and washed with phosphate-buffered saline (PBS) once, and images were taken using Zeiss Axio Observer.A1 microscope and processed using Axios Vision LE software.

Human tissue

All patients were consented before surgery for tissue collection protocol, and patient-derived tissues were obtained fresh or were paraffin-embedded according to approved institutional review board protocol. High-grade serous OvCa tumor samples were obtained from patients with clinical stage III and IV disease (International Federation of Gynecology and Obstetrics) undergoing primary debulking surgery at the University of Chicago hospital. For adipocyte co-culture experiments, human omental tissues were obtained from patients with benign, non-cancer-related conditions (for example, incontinence and fibroids).

Mouse studies

Intraperitoneal xenograft experiments were performed by injecting SKOV3i1p1 (5 million cells per mouse) or HeyA8-luciferase (1 million cells per mouse) cells into female immunocompromised athymic nude mice (Harlan Envigo, HSD: athymic nude), and tumor burden determined after 4 and 2 weeks post injection, respectively[5]. Tumor burden in mice injected with GPAT3 knockdown cells was assessed by injecting 100 µl D-luciferin (30 mg ml^{-1}) 10 min before imaging using the in vivo imaging system (IVIS) spectrum in vivo imaging system. Image analysis was carried out using live Image 4.4 software. For the in vivo [^{13}C]-glucose tracing experiment, 5 million stable SKOV3ip1 cells (transduced with either control shRNA or shRNA targeting HIF1α) were injected into female athymic nude mice (Harlan Envigo, HSD: athymic nude), and tumors were allowed to establish for 4 weeks. Mice were injected three times with 1.34 mM [^{13}C]-glucose solution in PBS (80 µl)

at 15 min intervals. Omental tumors were excised and snap frozen in liquid nitrogen. Of note we did not observe ascites formation by the end point of our xenograft experiments. All animal studies were approved by the Institutional Animal Care and Use Committee at the University of Chicago (protocol #71951). Animals were housed in standard breeding cages, maintained at 20–26 °C, relative humidity of 50% (±20%), with 12 h light and dark cycles. Food and water were provided ad libitum.

[^{13}C]-glucose tracing analysis

Glucose enrichment analysis on human omental explant tissues (from three patients with high-grade serous ovarian cancer (HGSOC), three sections were analyzed from each tumor) and mouse omental tissues was carried out as described previously[26,42]. Omental tumor biopsies from patients with HGSOC were sectioned (0.5–1 mm) and incubated in DMEM supplemented with 10 mM [U-^{13}C]-glucose (Cambridge Isotope Laboratories) and 2 mM glutamine. Explants were incubated for 24 h in an incubator maintained at 37 °C with 5% CO_2, with gentle rocking. Metabolites from mouse omentum isolated from xenograft experiments (as described above) and ex vivo cultures of human omental tumors were extracted using 80% cold methanol. Protein estimation was carried out using a bicinchoninic acid (BCA) assay (Pierce, Thermo Scientific), and equal protein amounts were dried using a speed-vac. Data acquisition was performed by reverse-phase chromatography on a 1290 UHPLC LC system interfaced to a high-resolution MS 6550 iFunnel Q-TOF mass spectrometer (Agilent Technologies). The mass spectrometer was operated in positive and negative electrospray ionization modes (ESI+ and ESI−). Analytes were separated on an Acquity UPLC HSS T3 column (1.8 µm, 2.1 × 150 mm, Waters). The column was kept at room temperature. Mobile phase A composition was 0.1% formic acid in water, and mobile phase B composition was 0.1% formic acid in 100% acetonitrile. The LC gradient was 0 min: 1% B; 5 min: 5% B; 15 min: 99% B; 23 min: 99% B; 24 min: 1% B; 25 min: 1% B. The flow rate was 250 µl min^{-1}. The sample injection volume was 5 µl. ESI source conditions were set as follows: dry gas temperature 225 °C and flow 18 l min^{-1}, fragmentor voltage 175 V, sheath gas temperature 350 °C and flow 12 l min^{-1}, nozzle voltage 500 V, and capillary voltage +3,500 V in positive mode and −3,500 V in negative. The instrument was set to acquire over the full m/z range of 40–1,700 in both modes, with the MS acquisition rate of 1 spectrum s^{-1} in profile format. Raw data files (.d) were processed using Profinder B.08.00 SP3 software (Agilent Technologies) with an in-house database containing retention time and accurate mass information on 600 standards from Mass Spectrometry Metabolite Library (IROA Technologies), which was created under the same analysis conditions. The in-house database matching parameters were mass tolerance 10 ppm, retention time tolerance 0.5 min and co-elution coefficient 0.5. The peak integration result was manually curated in Profinder for improved consistency and exported as a spreadsheet (.csv).

For tracing the flow of glucose-derived carbons into G3P, SKOV3ip3 cells were treated with control medium or Adi CM for 6 h. Cells were washed with PBS and cultured in 10 mM [U-^{13}C]-glucose for 1 h. Metabolites were extracted using 80% cold methanol, subjected to three freeze–thaw cycles and centrifuged for 30 min at 16,000g. The supernatants were evaporated using a speed-vac, the pellet was suspended in 40 µl anhydrous pyridine and derivatized by heating samples at 70 °C in tube containing 80 µl *N*-(*tert*-butyldimethylsilyl)-*N*-methyltrifluoroacetamide. The samples were analyzed using an Agilent 6890 gas chromatography mass spectrometer coupled to Agilent 5973N mass selective detector, to determine the total pool of G3P and the relative contributions of ^{13}C and ^{12}C (ref. 43).

Metabolomic analysis

Primary omental adipocytes isolated from seven consenting patients were co-cultured with SKOV3ip1 cells for 18 h (1:5 PCV, adipocytes: DMEM/F12 media), after which adipocytes, cancer cells and media were collected for metabolomic analysis. Equal number of cells and an equal volume of media were aliquoted for analysis. Sample extraction and untargeted metabolomics analysis of primary metabolites and complex lipids were carried out as previously described[44,45]. Analysis of oxylipins, endocannabinoids and ceramides (in the media) were constructed using gas chromatography and LC–MS platforms[46,47] at the West Coast Metabolomics Center, University of California, Davis.

Microarray analysis

SKOV3ip1 cells were co-cultured with primary omental adipocytes for 8 h. Cancer cells and adipocytes were separated and washed several times with PBS. Cells were lysed using TRIzol (Life Technologies), and total RNA was isolated according to the manufacturer's protocol using RNeasy kit (Qiagen), following in column DNase treatment. Microarray analysis was carried out using the Illumina BeadChipHT-12v4 expression array as previously described[5]. Data processing was carried out using Illumina Genome studio v2011.1 and Partek Genomics suite v6.6. Average signal intensities were background subtracted, $\log_2$ transformed and quantile normalized. Customized data processing scripts were developed in R version 3.3.0. Each experimental group had three replicates, and differentially expressed genes were identified as genes with a q-value of 0.05 and a fold change of 2 and above.

Proteomic analysis

SKOV3ip1 cells transduced with either control or HIF1α targeting shRNA were co-cultured with human primary adipocytes for 16 h. Adipocytes were removed and cancer cells were trypsinized and frozen. Sample processing and MS was carried out as described by us previously[5]. A QExactive (Thermo Fisher Scientific) connected to EASY-nLC 1000 HPLC system (Thermo Fisher Scientific) was used for shotgun analysis. C18 particles of 1.9 µm were packed into 75-mm-inner-diameter, 50-cm-length columns, and samples were separated over a 250 min gradient from 2% to 60% (5 min to 5%, 180 min to 25%, 45 min to 35%, 20 min to 60%) in buffer B (80% acetonitrile and 0.5% formic acid) at 200 nl min^{-1}. High-energy collisional dissociation fragmentation was carried out at a normalized collision energy of 25, an isolation window of 2.2 Th, and a resolution of 17,500 at m/z 200. The top five intensity precursors were subjected to collision. Ion injections times were set to 20 ms (target value 3×10^6) and 120 ms (target value 1×10^5) for MS/MS scans. Data acquisition was carried out using Xcalibur software 4.1 and data analysis using Perseus software v1.6.15.0 (ref. 48). Missing values were imputed on the basis of normal distribution. A two-sided t-test was performed for pairwise comparisons, and significant proteins were identified using FDR of 0.05 and S_0 (within groups variance) of 0.1 (ref. 49).

MALDI IMS

Omental tumor samples were obtained from three patients with HGSOC. Samples were rinsed in physiological saline and immediately frozen and stored at −80 °C until analysis. Tissue sections (12 µm) were cut using a Leica CM1950 cryostat (Leica) and thaw mounted onto polylysine-coated ITO conductive slides. Slides were stored at −80 °C until analysis. The tissue sections were thawed under vacuum for 15 min before matrix application. Norharmane, a dual polarity matrix (7 mg ml^{-1} in $CHCl_3$:MeOH 70:30) was applied in eight layers (two layers at 5 µl min^{-1} followed by six layers at 10 µl min^{-1}) using a SunCollect (SunChrom) matrix spraying system (4 bar, 50 mm z-axis height). Tissue sections were dried under vacuum for 15 min before MALDI MSI data acquisition. MALDI MSI images were acquired using an EP-MALDI source[50] (Spectroglyph, LLC) equipped with a 349 nm laser (Spectra-Physics), coupled to an Orbitrap QExactive Plus (Thermo Scientific). The laser was set to 1.65 A and 500 Hz, the ion source pressure was 7.2 Torr; MSI pixel size was 35 × 35 µm. Mass spectra were acquired in the range of 150–2,000 m/z at 70,000 resolving power. Position files were aligned to the raw file using Image Insight (v. 0.1.0.11550,

Spectroglyph, LLC). We analyzed a total of 40 and 34 tissue regions (in the three tumor sections) composed of cancer cells adjacent and distant to the adipocytes, respectively.

IMS—image preprocessing and analysis

Raw spectra of the MSI dataset were converted into mzXML using RawConverter[51]. A modified version of the script ORBIIMAGEmzXML2Tricks (v. 0.10, G. Eijkel) was used to produce a basepeak spectrum from each MSI dataset. Basepeak spectra of all the samples were summed to obtain a global basepeak spectrum. Peak picking was then performed on the global basepeak spectrum, and the resulting peak list was used to extract the MS images from each sample's dataset using ORBIIMAGEmzXML2Tricks. MSI datacubes were imported into MATLAB R2019b (MathWorks) for image preprocessing and data analysis. Each MSI dataset was processed separately to remove peaks that negatively correlated with the tissue, each peak list was deisotoped, and the intensity of pixels outside the tissue was set to zero. A merged datacube was produced by selecting only those peaks that were detected in all tissue sections being compared and then using spatial offsets to place all datasets within the same coordinate space. The resulting datacube was total ion count normalized, and bright spots with an intensity over the 99.9th percentile were removed.

IMS—histological staining and annotation

Tissue sections were stained with hematoxylin and eosin (H&E) after MSI data acquisition. Briefly, residual MALDI matrix was removed with ethanol washes (2× 30 s each) followed by rehydration and H&E staining. Optical images of the histologically stained tissues were recorded using an Aperio CS2 scanner at 40× magnification (Aperio Technologies) and annotated using Aperio ImageScope (v 12.2.2.5015, Aperio Technologies). OvCa cells adjacent to adipocyte regions were defined as tumor cells closer than 200 µm to adipocytes; these tumor cells were shown to present intracellular lipid staining in a previous work[4]. OvCa cells further than 200 µm from adipocytes were annotated as distant from adipocytes. Histological images were imported in MATLAB and co-registered to the MALDI MSI dataset. Annotated regions were imported in MATLAB, converted into masks and aligned to the MSI dataset, to perform region-based analysis[52]. Region masks were merged together using the same spatial offsets of the MSI dataset to obtain a global mask that can be applied to all MSI images at once.

IMS—data analysis

ROC curve analysis was used to identify m/z that differentiate OvCa cells adjacent to adipocytes from those distant from adipocytes. ROC curve analysis was performed by comparing the $\log_2$-transformed intensities of the pixels. Only m/z features with a nonzero value in at least 30% of the pixels of the regions were considered for the analysis. To take into account any bias that may arise from the different dimensions of the regions, ROC analysis was performed on randomly selected pixels from the regions, using the number of pixels of the smallest area. ROC analysis was performed in MATLAB using the function perfcurve; ions corresponding to an AUC greater than 0.7 (increased intensity in OvCa cells adjacent to adipocytes) and lower than 0.3 (increased in OvCa cells distant from adipocytes) were selected. Selected m/z were assigned on the basis of the mass accuracy using METLIN[53] ($\Delta = 10$ ppm, $[M+H]^+$,$[M+Na]^+$,$[M+H-H_2O]^+$ adducts). Lipids are presented using the lipid species level notation[5,54].

Quantitative real-time reverse transcription PCR analysis

To determine the changes in mRNA expression, cancer cells were plated in six-well plates and allowed to attach for 36 h after which the medium was removed, cells washed with PBS (twice) and co-cultured with primary adipocytes (1:5 PCV ratio) for 12 h (ref. 6). Adipocytes were removed by pipetting, and cancer cells were washed with PBS (three to five times) to remove the remaining adipocytes. Cells were then lyzed using TRIzol (Life Technologies) and total RNA extracted (per manufacturer's protocol). Complementary DNA synthesis was carried out using 1 µg total RNA using high-capacity cDNA synthesis kit (Applied Biosystems). Subsequently, quantitative polymerase chain reaction (qPCR) was carried out using the 7500 Real-Time PCR System (Applied Biosystems) with probes for HK2 (Hs00606086_m1), GPAT3 (Hs00262010_m1), GPD1 (Hs01100039_m1) and normalized to GAPDH (Hs02758991_g1) as a loading control. Relative changes were calculated using $2^{-\Delta\Delta Ct}$ method, and a P value of <0.05 was considered significant (t-test).

Immunoblotting

Cell lysis was carried out using RIPA buffer supplemented with protease and phosphatase inhibitors. Subsequently, protein estimations were performed using BCA protein assay kit (Pierce, Thermo Scientific). Equal protein amounts were resolved on sodium dodecyl sulfate gels (4–20%), transferred onto nitrocellulose membrane, and blotted for antibodies against specific proteins HIF1α (BD Biosciences, cat. no. 610958, 1:1,000), HK-2 (Cell Signaling Technology, cat. no. 2867, 1:1,000), p-STAT3 Tyr 708 (Cell Signaling Technology, cat. no. 9131, 1:1,000), total STAT3 (Cell Signaling Technology, cat. no. 9139, 1:1,000), GAPDG (Cell Signaling Technology, cat. no. 5174, 1:1,000) and β-actin (Millipore Sigma, cat. no. A5441, 1:3,000).

Immunohistochemistry

Immunohistochemistry was carried out as previously discussed[4]. Serial sections of omental tumors from patients with HGSOC were stained using antibodies against HIF1α (BD Biosciences, cat. no. 610958, 1:50), HK2 (Cell Signaling Technology, cat. no. 2867, 1:50), GPAT3 (Novus, cat. no. NBP-1-93629, 1:250), Ki-67 (Thermo Scientific Labvision, cat. no. RM-9160, 1:400), cleaved caspase 3 (Cell Signaling Technology, cat. no. 9661, 1:200) and 4-HNE (Abcam cat. no. ab46545, 1:300).

Lentivirus production and RNA interference

293T cells were transfected with packaging plasmids (8 µg of pCMV-dR8.2 dVPR and 1 µg pCMV-VSV-G, a gift from Robert Weinberg, Addgene plasmid #8455 and 8454, respectively) along with shRNA plasmids (8 µg) using Lipofectamine 2000 (Thermo Fisher Scientific) transfection reagent. Viral supernatants were collected 48 h after transfection and added to cell lines after filtration using 0.45 µm syringe filters. Cancer cell lines were transduced with lentivirus containing shRNA targeting HIF1α (TRCN0000003810) and GPAT3 (TRCN0000162335) to generate stable lines.

Omental explant assay

Human omental tissue was collected and ex-vivo culture carried out[5] to determine the effect of HIF1α knockdown on the colonization capacity OvCa cells. Then 10 mm punch biopsies of omental tissue (three per group) were added to a 24-well ultralow-attachment plate. One million scramble/control or HIF1a targeting shRNA transduced SKOV3ip1 cells were stained using CellTracker Red CMTPX Dye (Thermo Fisher Scientific) and added to each well. After 18 h (adhesion) and 72 h (proliferation) culture, the cells were imaged using a Nikon Eclipse Ti2 microscope using a 4× objective. Subsequently, cancer cells were released from the tissue using trypsin and quantitated by measuring the fluorescence intensity (excitation 577 nm, emission 617 nm) using SpectraMax iD3 (Molecular Devices). The assay was repeated using tissue collected from three patients.

Bioenergetics: glycolysis and oxidative phosphorylation

The effect of adipocytes and HIF1α on glycolysis and oxidative phosphorylation was determined using the Seahorse XFe analyzer (Agilent) by measuring ECAR and oxygen consumption rate (OCR)[5,55]. Briefly, 10,000 cells were plated per well of 96-well Seahorse plates and allowed to attach overnight. Cells were treated with control media

or adipocyte-conditioned media for 18 h. Post treatment, cells were washed and either replaced with DMEM (D5030, Sigma-Aldrich) supplemented with glutamine (2 mM, Corning) for ECAR analysis or replaced with Seahorse DMEM base media (Agilent) supplemented with sodium pyruvate (1 mM, Corning), glucose (25 mM, Sigma-Aldrich) and glutamine (2 mM, Corning) for OCR analysis. The assay media pH was adjusted to 7.4. Cells were incubated in a non-CO_2 incubator for 1 h before the assay was started. For ECAR assays, sequential injection of glucose (10 mM, Sigma-Aldrich), oligomycin (2 µM, Sigma-Aldrich) and 2-deoxyglucose (50 mM, Sigma-Aldrich), and for OCR assays, sequential injection with oligomycin (1 µM, Sigma-Aldrich), FCCP (carbonyl cyanide 4-(trifluoromethoxy)phenylhydrazone) (1 µM, Sigma-Aldrich), antimycin A (1 µM, Sigma-Aldrich) and rotenone (1 µM, Sigma-Aldrich) was carried out. Background-corrected rate data were plotted to determine changes in ECAR and OCR levels.

Luciferase activity assay—HIF1α stability assay

To quantitatively measure the effect of adipocyte CM HIF1α stability, we transfected SKOV3ip1 and OVCAR5 cells with ODD-luciferase-pcDNA3 construct (a kind gift from William Kaeline, Addgene plasmid #18965) and generated stable lines[17]. These stable cells were plated in six-well plates, allowed to attach for 36 h, and treated with either control medium or adipocyte CM in triplicate for 6 h. Cells were subsequently lysed using reporter lysis buffer (Promega), and luciferase activity was measured using an illuminometer (Lumat LB 9507, Berthold Technology). Data were normalized to protein levels using a BCA kit (Thermo Fisher Scientific).

MTT assay

Control shRNA and HIF1α transduced SKOV3ip1 cells were plated in 96-well plates (3,000 per well) and allowed to attach. The cells were treated with control medium (DMEM/F12 medium with 1% streptomycin and 1% penicillin) or primary human omental Adi CM for 18 h. Subsequently, cells were treated with RSL3 (1 µM), ferrostatin-1 (1 µM) and zVAD-fmk (10 µM) and incubated for an additional 6 h. At the end of 24 h, (3-(4,5-dimethylthiazol-2-yl)-2,5-diphenyl-2H-tetrazolium bromide) (MTT) assay was carried out as described before[5]. Relative percent cell viability was calculated on the basis of the values from control medium-treated group (Csh − Adi control and Hsh − Adi control).

Lipid peroxidation assay—MDA

To determine the intracellular levels of MDA, thiobarbituric acid reactive substance assay was carried out (using TBARS assay kit, Cayman) as described previously[5]. Control shRNA and HIF1α transduced SKOV3ip1 cells were plated in 15 cm dishes and co-cultured with primary adipocytes (1:5 PCV adipocytes:medium) for 18 h, following which, cell pellets were sonicated and boiled, and assay was carried out as per manufacturer's protocol.

Lipid ROS measurement—C11 Bodipy 581/591

OvCa cells (control shRNA and HIF1α transduced SKOV3ip1 cells) were plated in black-walled 96-well plates (3,000 per well) and allowed to attach. The cells were subsequently treated with either control medium or Adi CM in the presence of (2 µM) C11 Bodipy 581/591 dye (Thermo Fisher Scientific) and images were taken every 2 h at 10× magnification using Incucyte S3 live cell imaging system (Sartorius). Cells were continuously imaged for 24 h, and the hourly mean total integrated fluorescent intensity measured using the green channel (excitation 441–481 nm, emission 503–544 nm) was plotted for each group.

Statistical analysis and reproducibility

GraphPad Prism 7 software was used to calculate statistical significance. Data are presented as mean ± standard error of the mean (s.e.m.), and unless otherwise stated, a two-tailed Student's *t*-test was used to determine statistical significance; a *P* value less than 0.05 was considered significant. Unless stated, experiments were repeated three times, and one representative experiment is shown. For metabolomic analyses, a mixed-effects one-way ANOVA was carried out. Metabolites with a *P* value of <0.5 were considered significantly changed, and directional changes were depicted as network maps generated using Cytoscape 2.0. Significantly altered metabolites and genes were integrated to obtain a multi-omics dataset. Gene and metabolite pathway over-representation analysis was performed using Integrated Molecular Pathway Level Analysis (IMPaLA)[56]. Enriched pathways were identified on the basis of FDR and adjusted *P* values ≤0.05. Hierarchical clustering of enriched pathways was subsequently carried out to identify significant networks and visualized using Kyoto Encyclopedia of Genes and Genomes pathways.

Reporting summary

Further information on research design is available in the Nature Portfolio Reporting Summary linked to this article.

Data availability

Metabolomic data are deposited in the metabolomics workbench (https://www.metabolomicsworkbench.org/) and can be queried using the project https://doi.org/10.21228/M82S3K. Raw and processed microarray data are available in the Gene Expression Omnibus database (accession number GSE235641). Unique biological materials will be provided upon reasonable request. Source data are provided with this paper.

References

1. Lengyel, E., Makowski, L., DiGiovanni, J. & Kolonin, M. G. Cancer as a matter of fat: the crosstalk between adipose tissue and tumors. *Trends Cancer* **4**, 374–384 (2018).
2. Mukherjee, A., Bilecz, A. J. & Lengyel, E. The adipocyte microenvironment and cancer. *Cancer Metastasis Rev.* https://doi.org/10.1007/s10555-022-10059-x (2022).
3. Eckert, M. A. et al. Genomics of ovarian cancer progression reveals diverse metastatic trajectories including intraepithelial metastasis to the fallopian tube. *Cancer Discov.* **6**, 1342–1351 (2016).
4. Nieman, K. M. et al. Adipocytes promote ovarian cancer metastasis and provide energy for rapid tumor growth. *Nat. Med.* **17**, 1498–1503 (2011).
5. Mukherjee, A. et al. Adipocyte-induced FABP4 expression in ovarian cancer cells promotes metastasis and mediates carboplatin resistance. *Cancer Res.* **80**, 1748–1761 (2020).
6. Ladanyi, A. et al. Adipocyte-induced CD36 expression drives ovarian cancer progression and metastasis. *Oncogene* **37**, 2285–2301 (2018).
7. Lunt, S. Y. & Vander Heiden, M. G. Aerobic glycolysis: meeting the metabolic requirements of cell proliferation. *Annu. Rev. Cell Dev. Biol.* **27**, 441–464 (2011).
8. Fagone, P. & Jackowski, S. Membrane phospholipid synthesis and endoplasmic reticulum function. *J. Lipid Res.* **50**, S311–S316 (2009).
9. Engelmann, B. & Wiedmann, M. K. Cellular phospholipid uptake: flexible paths to coregulate the functions of intracellular lipids. *Biochim. Biophys. Acta* **1801**, 609–616 (2010).
10. Schug, Z. T. et al. Acetyl-CoA synthetase 2 promotes acetate utilization and maintains cancer cell growth under metabolic stress. *Cancer Cell* **27**, 57–71 (2015).
11. Takeuchi, K. & Reue, K. Biochemistry, physiology, and genetics of GPAT, AGPAT, and lipin enzymes in triglyceride synthesis. *Am. J. Physiol. Endocrinol. Metab.* **296**, E1195–E1209 (2009).
12. Buescher, J. M. et al. A roadmap for interpreting ^{13}C metabolite labeling patterns from cells. *Curr. Opin. Biotechnol.* **34**, 189–201 (2015).

13. Favaro, E. et al. Glucose utilization via glycogen phosphorylase sustains proliferation and prevents premature senescence in cancer cells. *Cell Metab.* **16**, 751–764 (2012).
14. Chen, H, C. et al. Hypoxia induces a metabolic shift and enhances the stemness and expansion of cochlear spiral ganglion stem/progenitor cells. *Biomed. Res. Int.* **2015**, 359537 (2015).
15. Sumi, C. et al. Suppression of mitochondrial oxygen metabolism mediated by the transcription factor HIF-1 alleviates propofol-induced cell toxicity. *Sci. Rep.* **8**, 8987 (2018).
16. Laurent, V. et al. Periprostatic adipose tissue favors prostate cancer cell invasion in an obesity-dependent manner: role of oxidative stress. *Mol. Cancer Res.* **17**, 821–835 (2019).
17. Hart, P. C. et al. Mesothelial cell HIF1α expression is metabolically downregulated by metformin to prevent oncogenic tumor–stromal crosstalk. *Cell Rep.* **29**, 4086–4098 e4086 (2019).
18. Safran, M. et al. Mouse model for noninvasive imaging of HIF prolyl hydroxylase activity: assessment of an oral agent that stimulates erythropoietin production. *Proc. Natl Acad. Sci. USA* **103**, 105–110 (2006).
19. Coscia, F. et al. Multi-level proteomics identifies CT45 as mediator of chemosensitivity and immunotherapy target in ovarian cancer. *Cell* **175**, 159–170 (2018).
20. Williamson, J. R. et al. Hyperglycemic pseudohypoxia and diabetic complications. *Diabetes* **42**, 801–813 (1993).
21. Walter, M., Liang, S., Ghosh, S., Hornsby, P. J. & Li, R. Interleukin 6 secreted from adipose stromal cells promotes migration and invasion of breast cancer cells. *Oncogene* **28**, 2745–2755 (2009).
22. Lengyel, E. Ovarian cancer development and metastasis. *Am. J. Pathol.* **177**, 1053–1064 (2010).
23. Yang, W. S. & Stockwell, B. R. Ferroptosis: death by lipid peroxidation. *Trends Cell Biol.* **26**, 165–176 (2016).
24. Yang, W. S. et al. Regulation of ferroptotic cancer cell death by GPX4. *Cell* **156**, 317–331 (2014).
25. Dixon, S. J. et al. Ferroptosis: an iron-dependent form of nonapoptotic cell death. *Cell* **149**, 1060–1072 (2012).
26. Lane, A. N., Yan, J. & Fan, T. W. ^{13}C tracer studies of metabolism in mouse tumor xenografts. *Bio Protoc.* https://doi.org/10.21769/bioprotoc.1650 (2015).
27. Scott, A. J. et al. Norharmane matrix enhances detection of endotoxin by MALDI–MS for simultaneous profiling of pathogen, host, and vector systems. *Pathog. Dis.* https://doi.org/10.1093/femspd/ftw097 (2016).
28. Natsume, M. et al. Omental adipocytes promote peritoneal metastasis of gastric cancer through the CXCL2–VEGFA axis. *Br. J. Cancer* **123**, 459–470 (2020).
29. Haverkamp, L., Brenkman, H. J., Ruurda, J. P., Ten Kate, F. J. & van Hillegersberg, R. The oncological value of omentectomy in gastrectomy for cancer. *J. Gastrointest. Surg.* **20**, 885–890 (2016).
30. Bristow, R. E., Tomacruz, R. S., Armstrong, D. K., Trimble, E. L. & Montz, F. J. Survival effect of maximal cytoreductive surgery for advanced ovarian carcinoma during the platinum era: a meta-analysis. *J. Clin. Oncol.* **20**, 1248–1259 (2002).
31. Hosios, A. M. et al. mTORC1 regulates a lysosome-dependent adaptive shift in intracellular lipid species. *Nat. Metab.* https://doi.org/10.1038/s42255-022-00706-6 (2022).
32. Szachowicz-Petelska, B. et al. Phospholipid composition and electric charge in healthy and cancerous parts of human kidneys. *J. Membr. Biol.* **246**, 421–425 (2013).
33. Dobrzynska, I., Szachowicz-Petelska, B., Sulkowski, S. & Figaszewski, Z. Changes in electric charge and phospholipids composition in human colorectal cancer cells. *Mol. Cell. Biochem.* **276**, 113–119 (2005).
34. Piccolis, M. et al. Probing the global cellular responses to lipotoxicity caused by saturated fatty acids. *Mol. Cell* **74**, 32–44 e38 (2019).
35. Listenberger, L. L. et al. Triglyceride accumulation protects against fatty acid-induced lipotoxicity. *Proc. Natl Acad. Sci. USA* **100**, 3077–3082 (2003).
36. Petschnigg, J. et al. Good fat, essential cellular requirements for triacylglycerol synthesis to maintain membrane homeostasis in yeast. *J. Biol. Chem.* **284**, 30981–30993 (2009).
37. Barrera, G. Oxidative stress and lipid peroxidation products in cancer progression and therapy. *ISRN Oncol.* **2012**, 137289 (2012).
38. Yang, M. et al. Clockophagy is a novel selective autophagy process favoring ferroptosis. *Sci. Adv.* **5**, eaaw2238 (2019).
39. Zou, Y. et al. Plasticity of ether lipids promotes ferroptosis susceptibility and evasion. *Nature* **585**, 603–608 (2020).
40. Mukherjee, A. Isolation of primary normal and cancer-associated adipocytes from the omentum. *Mol. Biol.* **2424**, 167–175 (2022).
41. Mitra, A. K. et al. MicroRNAs reprogram normal fibroblasts into cancer-associated fibroblasts in ovarian cancer. *Cancer Discov.* **2**, 1100–1108 (2012).
42. Sellers, K. et al. Pyruvate carboxylase is critical for non-small-cell lung cancer proliferation. *J. Clin. Invest.* **125**, 687–698 (2015).
43. Faubert, B. et al. Lactate metabolism in human lung tumors. *Cell* **171**, 358–371 e359 (2017).
44. Kind, T. et al. Fiehnlib: mass spectral and retention index libraries for metabolomics based on quadrupole and time-of-flight gas chromatography/mass spectrometry. *Anal. Chem.* **81**, 10038–10048 (2009).
45. Meissen, J. K. et al. Induced pluripotent stem cells show metabolomic differences to embryonic stem cells in polyunsaturated phosphatidylcholines and primary metabolism. *PLoS ONE* **7**, e46770 (2012).
46. Olmstead, K. I. et al. Insulin induces a shift in lipid and primary carbon metabolites in a model of fasting-induced insulin resistance. *Metabolomics* https://doi.org/10.1007/s11306-017-1186-y (2017).
47. Agrawal, K. et al. Effects of atopic dermatitis and gender on sebum lipid mediator and fatty acid profiles. *Prostaglandins Leukot. Essent. Fat. Acids* **134**, 7–16 (2018).
48. Tyanova, S. et al. The Perseus computational platform for comprehensive analysis of (prote)omics data. *Nat. Methods* **13**, 731–740 (2016).
49. Tusher, V. G., Tibshirani, R. & Chu, G. Significance analysis of microarrays applied to the ionizing radiation response. *Proc. Natl Acad. Sci. USA* **98**, 5116–5121 (2001).
50. Belov, M. E. et al. Design and performance of a novel interface for combined matrix-assisted laser desorption ionization at elevated pressure and electrospray ionization with orbitrap mass spectrometry. *Anal. Chem.* **89**, 7493–7501 (2017).
51. He, L., Diedrich, J., Chu, Y. Y. & Yates, J. R. 3rd Extracting accurate precursor information for tandem mass spectra by RawConverter. *Anal. Chem.* **87**, 11361–11367 (2015).
52. Greco, F. et al. Mass spectrometry imaging as a tool to investigate region specific lipid alterations in symptomatic human carotid atherosclerotic plaques. *Metabolites* https://doi.org/10.3390/metabo11040250 (2021).
53. Smith, C. A. et al. METLIN: a metabolite mass spectral database. *Ther. Drug Monit.* **27**, 747–751 (2005).
54. Liebisch, G. et al. Shorthand notation for lipid structures derived from mass spectrometry. *J. Lipid Res.* **54**, 1523–1530 (2013).
55. Curtis, M. et al. Fibroblasts mobilize tumor cell glycogen to promote proliferation and metastasis. *Cell Metab.* **29**, 141–155 e149 (2019).
56. Kamburov, A., Cavill, R., Ebbels, T. M., Herwig, R. & Keun, H. C. Integrated pathway-level analysis of transcriptomics and metabolomics data with IMPaLA. *Bioinformatics* **27**, 2917–2918 (2011).

Acknowledgements
We thank all patients at The University of Chicago for donating tissue to this study. We thank F. Coscia and M. Mann (Max Plank Institute of Biochemistry, Martinsried, Bavaria) for help with proteomic analysis, and J. Andrade at the Center for Research Informatics (University of Chicago) for assistance with microarray analysis. This work was supported by the Ann Sol Schreiber award (372898), Colleen's dream foundation and the DOD pilot award (W81XWH2110376) to A.M., NIH grants (R01CA169604, R35CA264619) awarded to E.L. D.B. is supported by NIH grant F31CA239330. R.J.D. is supported by grants from NIH (R35CA22044901) and by the Howard Hughes Medical Institute. We thank G. Isenberg for editing the paper. Figure 2b and Supplementary Figs. 2e,f, 5f and 6a,f were created using BioRender.com.

Author contributions
A.M. and E.L. supervised the study, and wrote and edited the paper. Data acquisition and analysis were carried out by all A.M., D.B., F.G., C.-Y.C., M.Z., T.S., H.S.V., B.F., M.T., J.F., D.G., M.R.L.F., J.W.N., O.F., R.J.D. and E.L. Adipocyte isolation, co-culture, Seahorse, gene and protein expression analysis (A.M. and C.-Y.C.), metabolomics (A.M., J.F., M.R.L.F., D.G. and T.S.), omics data integrations (D.G. and A.M.), IMS (F.G., A.M., L.A.M. and L.N.), [^{13}C]-glucose isotope tracing (A.M., D.B., H.S.V., B.F. and R.J.D.), xenograft studies (A.M.), animal studies (A.M., M.Z. and M.T.) and proteomics (A.M.). All authors edited and approved the final paper.

Competing interests
There are no potential conflicts of interest. E.L. received funding from Abbvie and Arsenal Bioscience for preclinical research studies unrelated to the submitted paper.

Additional information
Extended data is available for this paper at https://doi.org/10.1038/s42255-023-00879-8.

Supplementary information The online version contains supplementary material available at https://doi.org/10.1038/s42255-023-00879-8.

Correspondence and requests for materials should be addressed to Ernst Lengyel.

Peer review information *Nature Metabolism* thanks Rugang Zhang and the other, anonymous, reviewers for their contribution to the peer review of this work. Alfredo Giménez-Cassina, in collaboration with the *Nature Metabolism* team.

Reprints and permissions information is available at www.nature.com/reprints.

Publisher's note Springer Nature remains neutral with regard to jurisdictional claims in published maps and institutional affiliations.

https://doi.org/10.1038/s42255-023-00879-8

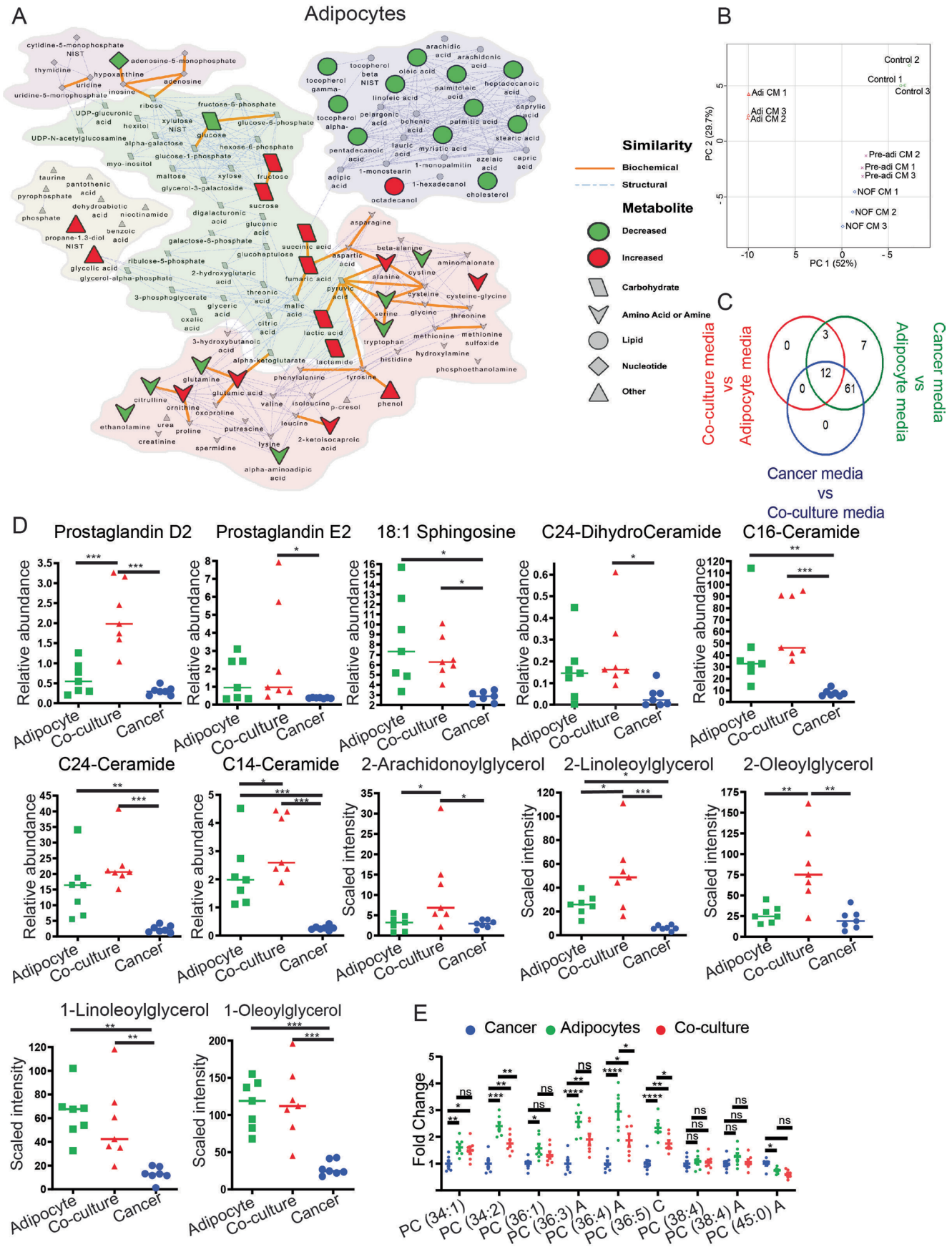

Extended Data Fig. 1 | See next page for caption.

https://doi.org/10.1038/s42255-023-00879-8

Extended Data Fig. 1 | Untargeted metabolomic analysis of adipocytes after co-culture with ovarian cancer cells. (a) Network map showing altered levels (red = increased; green = decreased) of biochemically and structurally similar metabolites in adipocytes after co-culture with SKOV3ip1 OvCa cells for 18 h. Biochemically and structurally similar metabolites are clustered. Metabolites in the same biochemical pathway are connected by orange lines. Structurally similar metabolites are connected by blue lines. **(b)** Principle component analysis (PCA) showing lipidomic changes in SKOV3ip1 cells induced by conditioned media derived from patient matched adipocytes (Adi CM), fibroblasts (NOF CM) and preadipocytes (Pre-adi CM). **(c)** Venn diagram showing number of metabolites altered in adipocytes, cancer cells, and co-culture derived media ($p < 0.05$, two-way ANOVA, mixed model post hoc Tukey HSD). **(d)** Changes in metabolites in adipocytes, cancer cells, and co-culture derived media. C24-ceramide, C16-ceramide and 18:1 sphingosine were primarily secreted by adipocytes; endocannabinoids such as 2-Arachidonylglycerol and 2-Linoleoylglycerol were increased in co-culture conditions ($p < 0.05$, one-way ANOVA). **(e)** Changes in phosphatidylcholine levels in the secretome of cancer cells (blue), adipocytes (green), and cancer cells co-cultured with adipocytes (red). Data extracted from metabolomics described in Fig. 1c. Statistical significance was calculated using two-way ANOVA, * $p < 0.05$, ** $p < 0.01$, *** $p < 0.001$.

https://doi.org/10.1038/s42255-023-00879-8

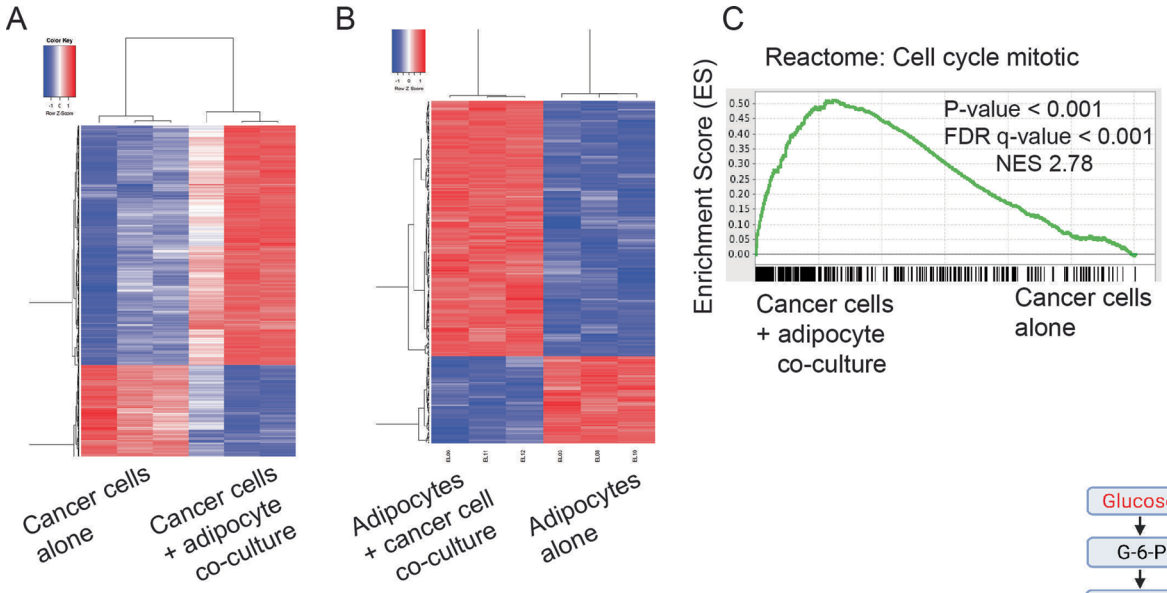

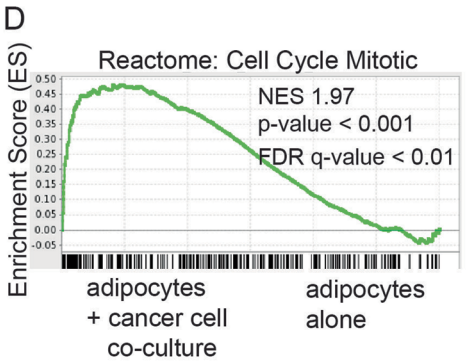

E

Gene	Fold change	q-value
GPAT3	2.26394	0.016627
AGPAT5	2.10369	0.0308767
PDK4	4.60221	0.0173085
LDHA	2.04013	0.0158894
LDHB	3.62299	0.0173249
MDH1	2.3726	0.0160187
SDHD	2.6942	0.0188857
ENO3	-2.71732	0.0158894

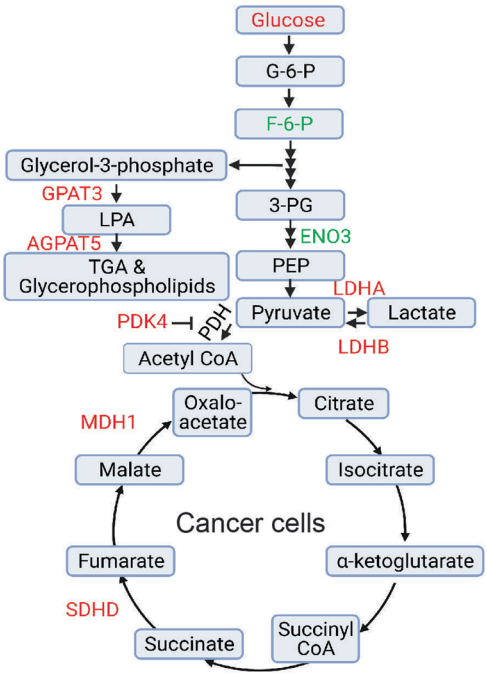

F

Gene name	Fold Change	q-vaue
PFKP	4.6353	0.00892773

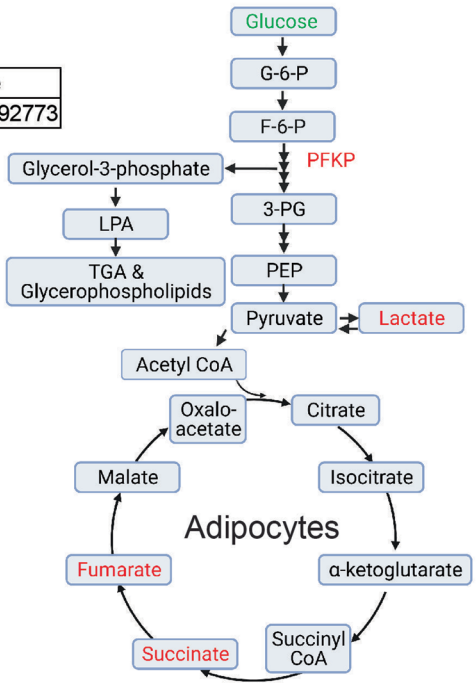

Extended Data Fig. 2 | See next page for caption.

https://doi.org/10.1038/s42255-023-00879-8

Extended Data Fig. 2 | Joint gene-metabolite analysis of adipocytes co-cultured with cancer cells. Gene expression analysis. Heat map showing clustering of **(a)** cancer cells +/− adipocyte co-culture, **(b)** adipocytes +/− co-culture with SKOV3ip1 cells for 12 h. Gene Set Enrichment Analysis (cell cycle) based on the gene expression (microarray) of **(c)** cancer cells +/− adipocyte co-culture and **(d)** adipocytes +/− SKOV3ip1 co-culture. (One-way ANOVA, FDR, q value < 0.05). Integration of gene expression and metabolites using IMPala, depicting changes in the **(e)** cancer cells +/− adipocyte co-culture and **(f)** adipocytes +/− co-culture with SKOV3ip1 cells. Genes and metabolites increased with co-culture are in red, those reduced are in green. Fold changes of significantly altered genes from microarray analysis are shown in a table on left (One-way ANOVA, FDR, q value < 0.05). (E, F Created with BioRender.com (2023)).

https://doi.org/10.1038/s42255-023-00879-8

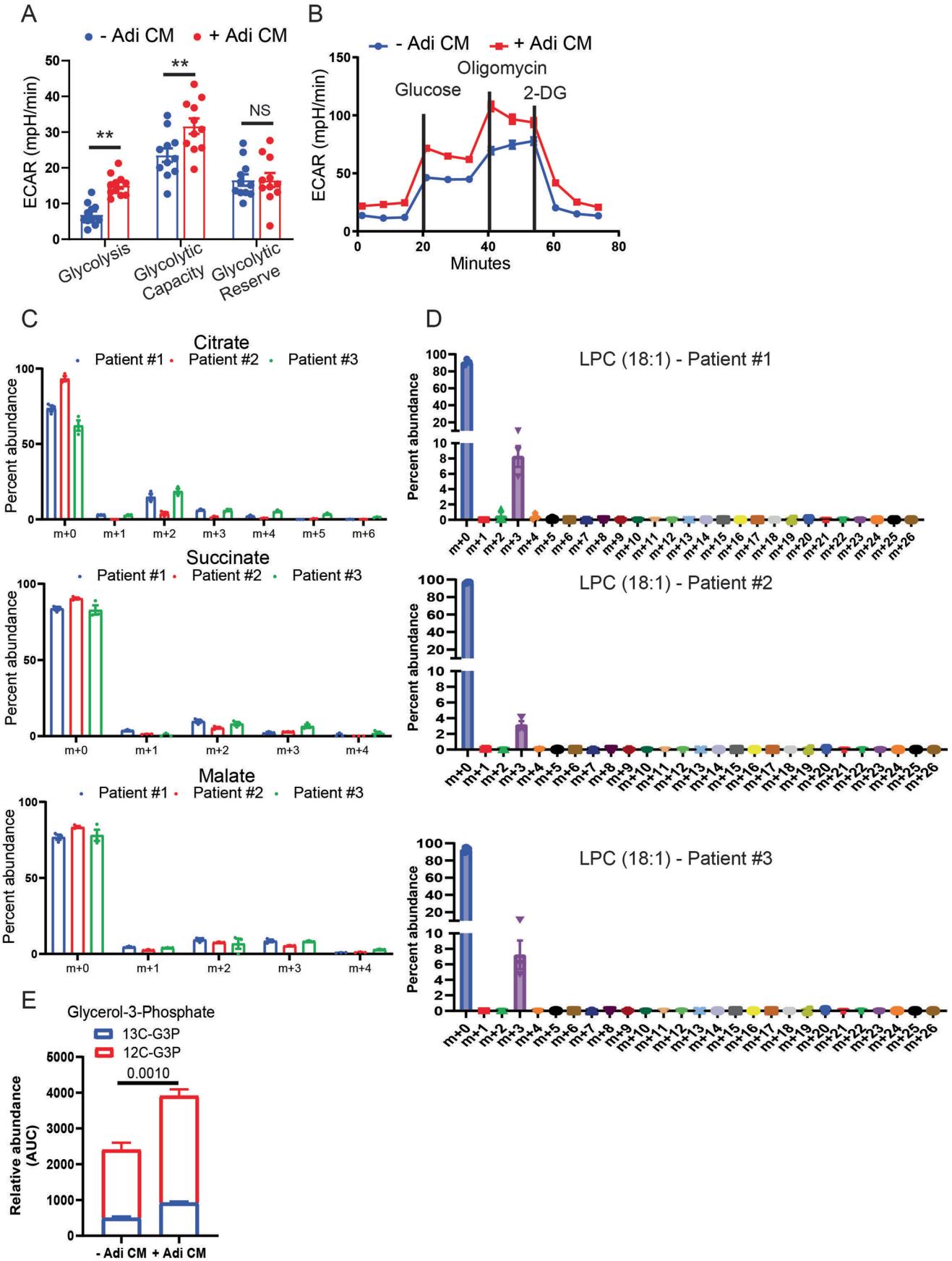

Extended Data Fig. 3 | See next page for caption.

https://doi.org/10.1038/s42255-023-00879-8

Extended Data Fig. 3 | Seahorse and metabolomics of ovarian cancer cells co-cultured with adipocytes. (a) Glycolytic (ECAR) profiles of SKOV3ip1 cells treated with adipocyte conditioned media (Adi CM) for 18 h measured using a Seahorse XF^{e}96 analyzer (n = 3 independent experiments, mean +/− SEM are plotted as bar graphs, two-way ANOVA, ** $p < 0.05$). **(b)** ECAR profile of OVCAR5 cells treated with Adi CM for 18 h (n = 3 independent experiments). **(c–d)**, *Ex-vivo* culture of omental tumor explants. Stable isotope tracing using [^{13}C]-glucose (data from Fig. 2c) for 24 h. Isotopologue prolife of (**C**) TCA cycle intermediates and (**D**) Lysophosphocholine (LPC) 18:1 for three patient tumors is plotted (n = 3 independent biological samples). Mean +/− SEM are plotted as bar graphs. (**e**) Stable isotope tracing. SKOV3ip1 cells were treated with either control or Adi CM for 6 h and glucose utilization traced using uniformly labeled [^{13}C]-glucose. Bar graph depict contribution of ^{13}C vs ^{12}C carbon to the total pool of glycerol-3-phosphate under specific treatment conditions (n = 3 independent experiments). Mean +/− SEM are plotted as bar graphs. ($p = 0.11$, two-way ANOVA; and $p = 0.001$ unpaired T-test).

https://doi.org/10.1038/s42255-023-00879-8

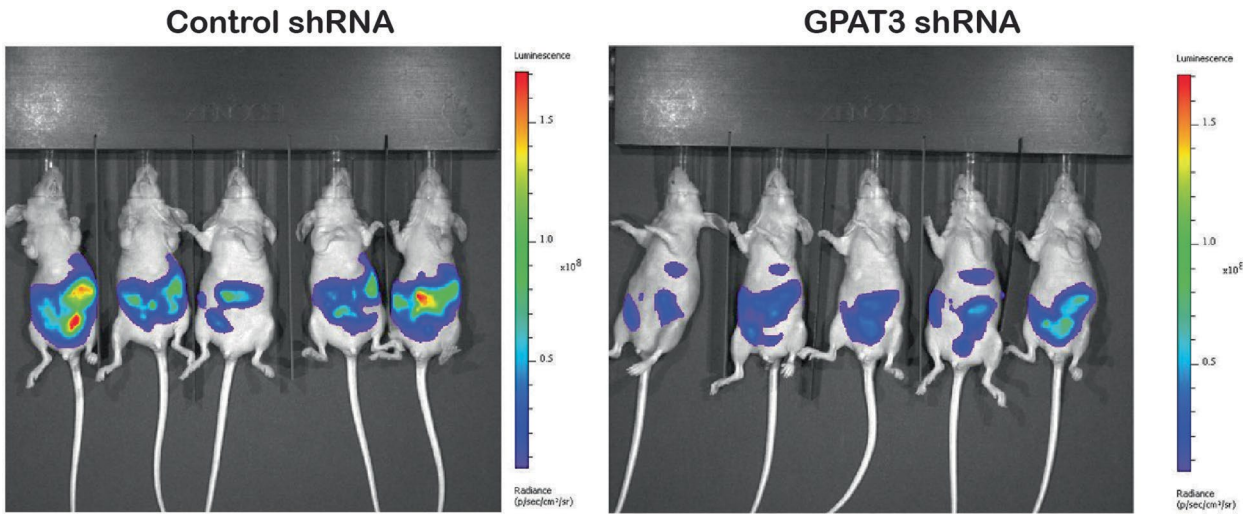

Extended Data Fig. 4 | Knockdown of GPAT3 reduces metastatic tumor burden in mice. Scrambled (Control shRNA) or GPAT3 targeting shRNA (GPAT3 shRNA) transduced, luciferase expressing, HeyA8 cancer cells were injected intraperitoneally into athymic nude mice and tumor burden visualized after 2 weeks using the IVIS spectrum *in vivo* imaging system. Images show end-point difference in tumor burden.

https://doi.org/10.1038/s42255-023-00879-8

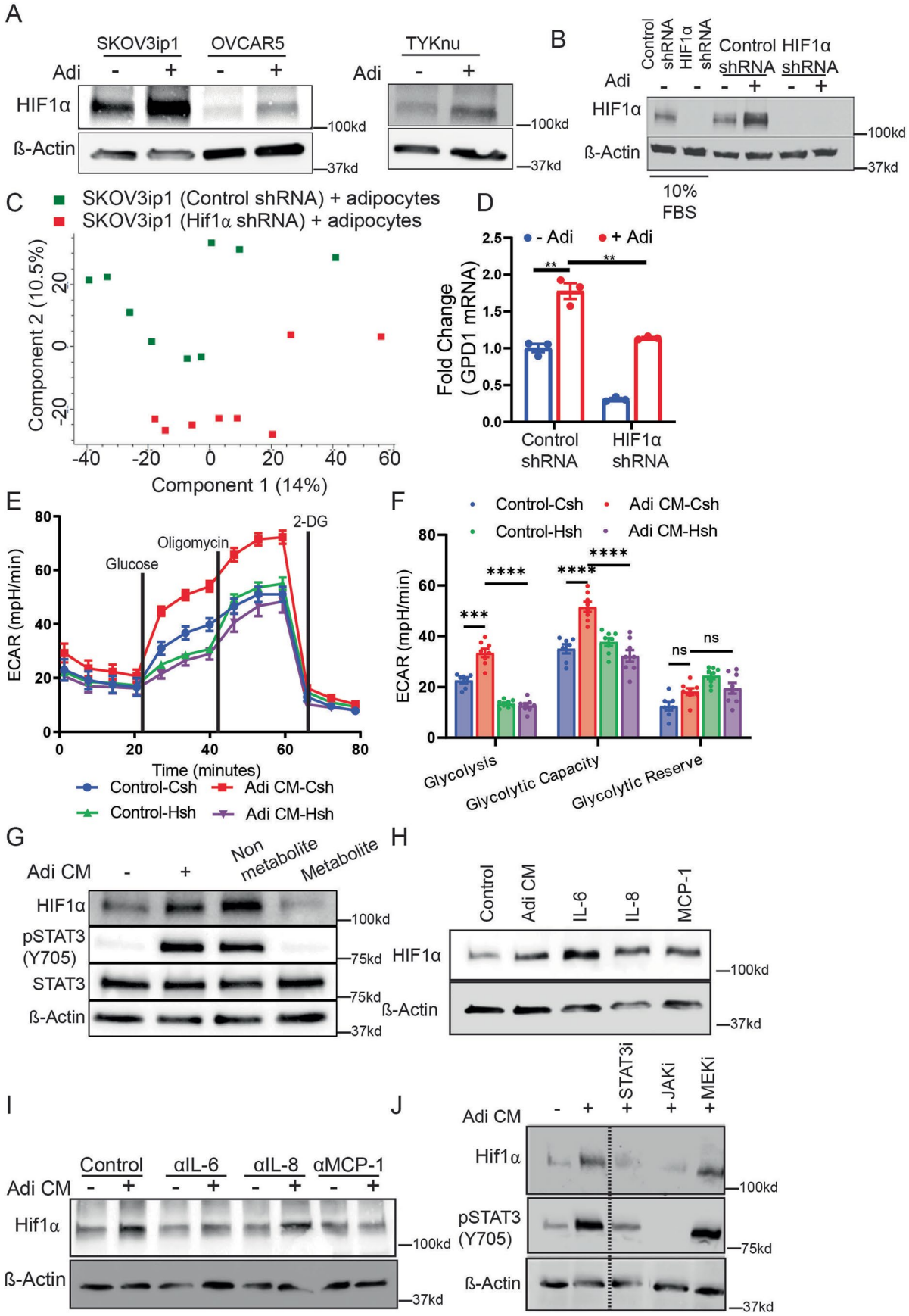

Extended Data Fig. 5 | See next page for caption.

https://doi.org/10.1038/s42255-023-00879-8

Extended Data Fig. 5 | Adipocyte-induced HIF1α regulates glycolysis. (a) Immunoblot of HIF1α in ovarian cancer cell lines co-cultured with Adi for 16 h (n = 3 independent experiments). (**b**) Immunoblot for HIF1α, showing stable knockdown of HIF1α in SKOV3ip1 cells (n = 3 independent experiments). **(c)** Principal component analysis using adipocyte co-cultured samples (16 h) stably expressing either control shRNA or HIF1α shRNA cells. (**d**) qPCR analysis to determine glycerol-3-phosphate dehydrogenase (GPD1) mRNA expression in stable HIF1α knockdown SKOV3ip1 cells after 12 h adipocyte co-culture. Mean +/− SEM are plotted as bar graphs. (n = 3 independent experiments, two-tailed t-test, ** $p < 0.005$). (**e-f**) SKOV3ip1 HIF1α knockdown cells were treated with Adi CM for 18 h, followed by Seahorse analysis to determine changes in ECAR (n = 3 independent experiments). (Mean +/− SEM, two-way ANOVA, *** $p = 0.0005$, **** $p < 0.0001$). **g**) Adi CM was fractioned into metabolite and non-metabolite fractions based on size (3 kd). SKOV3ip1 cells were treated with both fractions for 6 h and immunoblot carried out (n = 3 independent experiments). (**h**) Immunoblot for HIF1α after treatment of SKOV3i1p cells with 10 ng/ml of recombinant human cytokines (IL-6, IL-8, and MCP1) for 6 hr (n = 3 independent experiments. (**i**) Immunoblot of HIF1α expression in SKOV3ip1 cells treated with Adi CM (6 h) +/− neutralizing antibodies against human IL-6, IL-8, or MCP-1(n = 3 independent experiments. (**j**) SKOV3ip1 cells were pretreated with the STAT-3 inhibitor STATTIC (10 μM), the JAK2 inhibitor AZD-1480 (10 μM), or a MEK inhibitor, Trametinib (1 μM) for 30 min, followed by incubation with Adi CM for 6 h. Immunoblot of HIF1α expression (n = 3 independent experiments).

https://doi.org/10.1038/s42255-023-00879-8

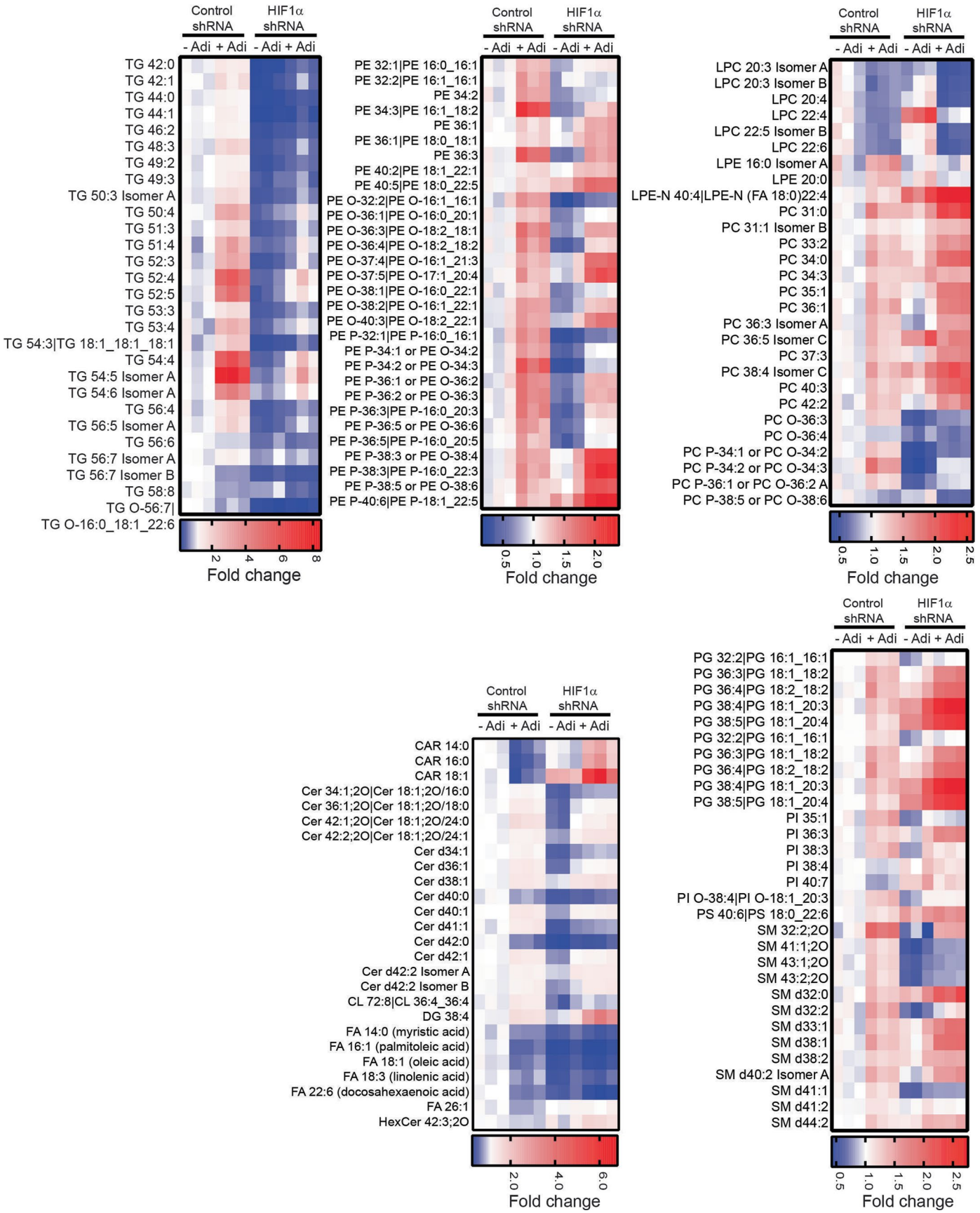

Extended Data Fig. 6 | See next page for caption.

https://doi.org/10.1038/s42255-023-00879-8

Extended Data Fig. 6 | Adipocyte-induced HIF1α alters the lipidome of ovarian cancer cells. Lipidomics. HIF1α shRNA or control shRNA transduced SKOV3ip1 cells were co-cultured with primary omental adipocytes for 18 h, and mass spectrometry performed. The heat map depicts fold changes of significantly altered lipids (two-tailed t-test, p value of <s0.05) with adipocyte co-culture and HIF1α knockdown. Lipids: Triacylglycerol, TG; Phosphatidylethanolamine, PE; Lysophosphatidylcholine, LPC; phosphatidylcholine, PC; carnitine, CAR; ceramide, Cer; fatty acid, FA; diacylglycerol, DG; phosphatidylglycerol, PG; phosphatidylinositol, PI; phosphatidylserine, PS; sphingomyelin, SM.

https://doi.org/10.1038/s42255-023-00879-8

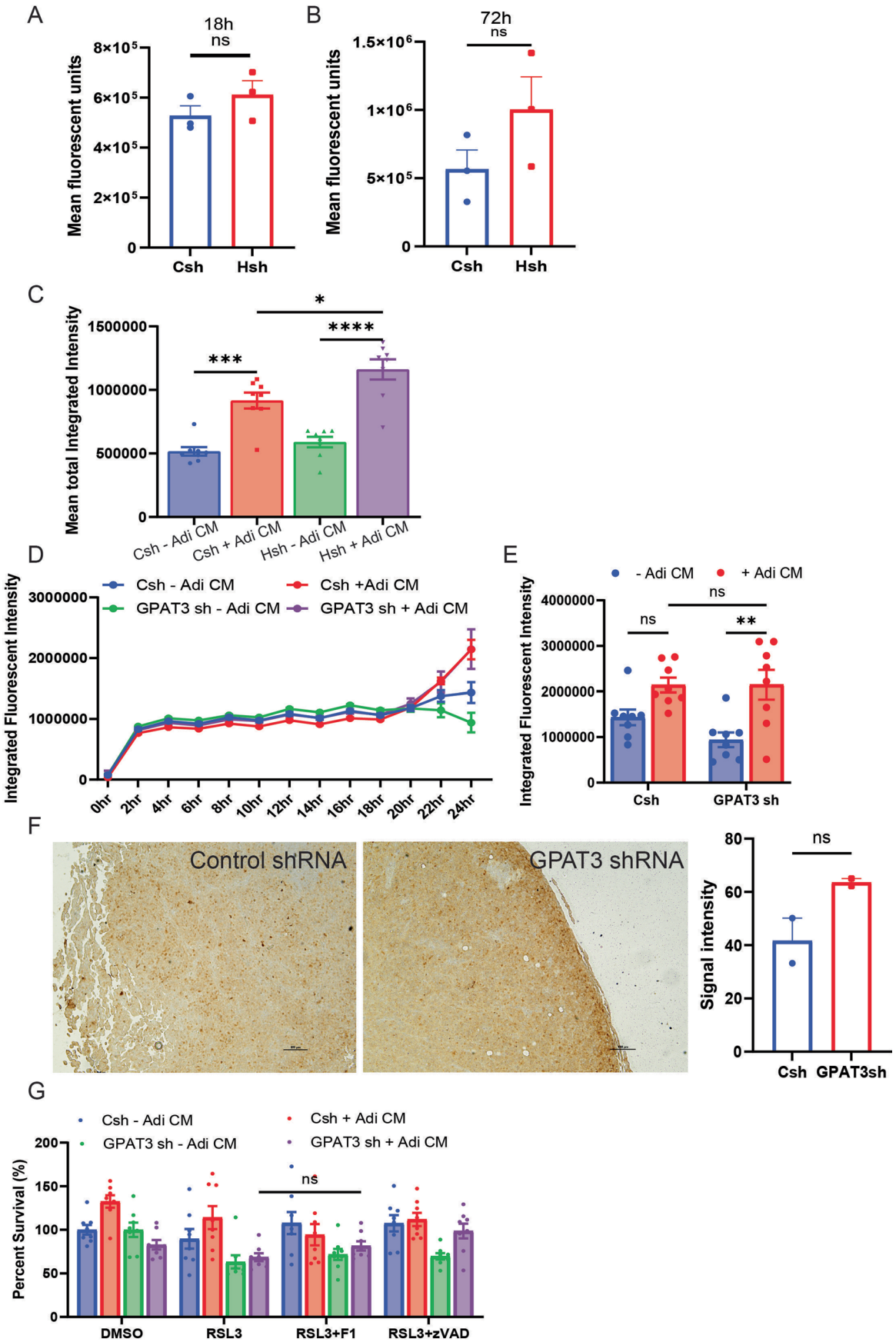

Extended Data Fig. 7 | See next page for caption.

https://doi.org/10.1038/s42255-023-00879-8

Extended Data Fig. 7 | Effect of HIF1α knockdown on ovarian cancer cells. **(a, b)** Explant assay. SKOV3ip1 cells transduced with either control shRNA or HIF1α shRNA were cultured with non-cancerous human omentum for (**A**) 18 h and (**B**) 72 h to measure cellular adherence capacity and proliferation, respectively (n = 3 biologically independent samples). Mean +/− SEM are plotted as bar graphs. (**c**) C11 Bodipy stained cells (control and HIF1α) were treated with adipocyte-derived conditioned media and mean fluorescent intensity measured after 24 h using Incucyte (data extracted from Fig. 5f). (n = 3 independent experiments, Mean +/− SEM are plotted as bar graphs, one-way ANOVA * $p < 0.05$, *** $p = 0.0002$, $p < 0.0001$.) (**D-E**) Lipid ROS measurements. HeyA8 cells transduced with either scrambled shRNA (Control shRNA) or GPAT3 shRNA was labelled with C11-Bodipy dye was treated adipocyte-derived conditioned media (Adi CM). (**d**) Images were taken every 2 h using Incucyte and total green fluorescence intensity plotted. (n = 3 independent experiments, Mean +/− SEM are plotted). (**e**) Bar graph depicts green fluorescence intensity measured at the 24 h time point. (n = 3 independent experiments, two-way ANOVA, ** $p = 0.003$, mean +/− SEM are plotted). (**f**) Immunohistochemistry for 4-HNE adducts in serial sections of xenograft omental tumors (from Fig. 3d). Staining intensities of the images (left) were quantified using ImageJ (right). (n = 3 independent experiments, two-tailed t-test, mean +/− SEM are plotted as bar graphs). (**g**) MTT assay to determine the viability of HeyA8 cells after treatment with the indicated compounds. (n = 3 independent experiments, two-way ANOVA, $p < 0.05$, mean +/− SEM are plotted as bar graphs).

nature portfolio

Corresponding author(s): Ernst Lengyel

Last updated by author(s): Jul 18, 2023

Reporting Summary

Nature Portfolio wishes to improve the reproducibility of the work that we publish. This form provides structure for consistency and transparency in reporting. For further information on Nature Portfolio policies, see our Editorial Policies and the Editorial Policy Checklist.

Statistics

For all statistical analyses, confirm that the following items are present in the figure legend, table legend, main text, or Methods section.

n/a	Confirmed	
☐	☒	The exact sample size (*n*) for each experimental group/condition, given as a discrete number and unit of measurement
☐	☒	A statement on whether measurements were taken from distinct samples or whether the same sample was measured repeatedly
☐	☒	The statistical test(s) used AND whether they are one- or two-sided *Only common tests should be described solely by name; describe more complex techniques in the Methods section.*
☒	☐	A description of all covariates tested
☐	☒	A description of any assumptions or corrections, such as tests of normality and adjustment for multiple comparisons
☐	☒	A full description of the statistical parameters including central tendency (e.g. means) or other basic estimates (e.g. regression coefficient) AND variation (e.g. standard deviation) or associated estimates of uncertainty (e.g. confidence intervals)
☐	☒	For null hypothesis testing, the test statistic (e.g. *F*, *t*, *r*) with confidence intervals, effect sizes, degrees of freedom and *P* value noted *Give P values as exact values whenever suitable.*
☒	☐	For Bayesian analysis, information on the choice of priors and Markov chain Monte Carlo settings
☒	☐	For hierarchical and complex designs, identification of the appropriate level for tests and full reporting of outcomes
☒	☐	Estimates of effect sizes (e.g. Cohen's *d*, Pearson's *r*), indicating how they were calculated

Our web collection on statistics for biologists contains articles on many of the points above.

Software and code

Policy information about availability of computer code

Data collection	Mass spectrometry based metabolomic data was acquired using the mass hunter software for Agilent systems and proteomic data was acuired using Xcalibur software 4.1. Microarry data was collected using GeneChip Command Console Software 4.0. Imaging mass spectrometry: Data Acquisition used two software packages, MALDI_Injector Ver 1.2.1.764 (Spectroglyph LLC, Kennewick, WA, USA) to control the MALDI imaging source, and Q Exactive Plus, version 2.8 SPI Build 2806 (ThermoFisher Scientific, Bremen, Germany) to control the Q Exactive Plus mass spectrometer. Axios Vision LE software was used to collect florescent images using the Zeiss Axio Observer.A1 microscope. IVIS spectrum in vivo imaging system used to collect live mouse bioluminescence signal.
Data analysis	Metabolomic data was analyzed using MSD chemStation F.01.03.2357 {GC MS) or Profinder B.08.00 (isotope tracing). Network maps were generated using Cytoscape 2.0. For microarray datasets analysis was performed using Illumina Genome studio v2011.1 and Partek Genomics suite v6.6. Gene set enrichment analysis was carried out using GSEA v2.2 software and gene set c2.cp.v5.l. Gene-metabolite over representation analysis was performed using IMPaLA (version 1). Imaging mass spectrometry: Merging of raw mass spectral data with position data, ImageInsight v.0.1.0.11550 (Spectroglyph LLC, Kennewick, WA, USA). Data analysis, Matlab R2019b (Mathworks, Natick, MA, USA).Seahorse data was analyzed using the Seahorse wave desktop software 2.6.0. Graph Pad Prism 7 was used for statistical analysis. Perseus software v1.6.15.0 was used for proteomic data analysis. Bioluminescence data was analyzed using live Image 4.4 software.

For manuscripts utilizing custom algorithms or software that are central to the research but not yet described in published literature, software must be made available to editors and reviewers. We strongly encourage code deposition in a community repository (e.g. GitHub). See the Nature Portfolio guidelines for submitting code & software for further information.

Data

Policy information about availability of data

All manuscripts must include a data availability statement. This statement should provide the following information, where applicable:

- Accession codes, unique identifiers, or web links for publicly available datasets
- A description of any restrictions on data availability
- For clinical datasets or third party data, please ensure that the statement adheres to our policy

Metabolomic data is available online (https://www.metabolomicsworkbench.org/data/DRCCMetadata.php?Mode=Project&ProjectID=PR000079) and can be accessed directly by Project DOI: 10.21228/M82S3K. Microarray data are available in the gene Expression Omnibus (GEO) database (Accession number: GSE235641). Both proteomic and microarray data is available as supplemental data.

Research involving human participants, their data, or biological material

Policy information about studies with human participants or human data. See also policy information about sex, gender (identity/presentation), and sexual orientation and race, ethnicity and racism.

Reporting on sex and gender	We studied ovarian cancer. Therefore, the data pertains to females (sex). Data on sex was collected during the patient's clinical visits. Segregated gender and sex data were not collected, and such analyses were not performed using patient data.
Reporting on race, ethnicity, or other socially relevant groupings	Given the small sample size of patient data, no socially relevant categorizations were performed.
Population characteristics	For adipose tissue consecutive patients were consented, de-indentified and no HPI data was collected. For tumor tissue collection, the average patient age was 62 years.
Recruitment	Informed consent was taken before enrollment of the patients in the tissue collection protocol. Consecutive patients were enrollment for primary tissue collection. There was no bias in patient enrollment.
Ethics oversight	Primary tissue collection protocol is approved by the University of Chicago's Institutional review board.

Note that full information on the approval of the study protocol must also be provided in the manuscript.

Field-specific reporting

Please select the one below that is the best fit for your research. If you are not sure, read the appropriate sections before making your selection.

☒ Life sciences ☐ Behavioural & social sciences ☐ Ecological, evolutionary & environmental sciences

For a reference copy of the document with all sections, see nature.com/documents/nr-reporting-summary-flat.pdf

Life sciences study design

All studies must disclose on these points even when the disclosure is negative.

Sample size	No statistical method/s were used to determine the sample size. Number of mice used for the studies were guided by previous experiments (PMID: 31043742 PMID: 32054768). In-vitro experiment sample size was based on the assay format and 'n" values have been provided in the figure legends.
Data exclusions	No data was excluded
Replication	All attempts at replication were successful. Experiments were repeated in triplicate, unless stated. For experiments in which primary cells were used, cell from multiple patients were used.
Randomization	Animals were not randomized for experiments. We study ovarian cancer and therefore used only female mice. All animals used were inbred lines, obtained from the same supplier, and were of identical age. In-vitro experiments had at least 3 technical repeats and were allocated into groups bases on experimental conditions.
Blinding	Investigators were blinded for animal experiments but were not blinded for other experiments due to feasibility issues.

Reporting for specific materials, systems and methods

We require information from authors about some types of materials, experimental systems and methods used in many studies. Here, indicate whether each material, system or method listed is relevant to your study. If you are not sure if a list item applies to your research, read the appropriate section before selecting a response.

Materials & experimental systems

n/a	Involved in the study
☐	☒ Antibodies
☐	☒ Eukaryotic cell lines
☒	☐ Palaeontology and archaeology
☐	☒ Animals and other organisms
☒	☐ Clinical data
☒	☐ Dual use research of concern
☒	☐ Plants

Methods

n/a	Involved in the study
☒	☐ ChIP-seq
☒	☐ Flow cytometry
☒	☐ MRI-based neuroimaging

Antibodies

Antibodies used

HIF1 (BD biosciences, cat# 610958, 1:1000), HK-2 (Cell Signaling Technology, cat# 2867, 1:1000), p-STAT3 Tyr 708 (Cell Signaling Technology, cat# 9131, 1:1000), total STAT3 (Cell Signaling Technology, cat# 9139, 1:1000), GAPDH(Cell Signaling Technology, cat# 5174, 1:1000), β-Actin (Millipore Sigma cat# A5441, 1:3000),), GPAT3 (Novus cat#NBP-1-93629, 1:250), Ki-67 (Thermo Scientific Labvision, Cat# RM-9160, 1:400), cleaved caspase 3 (Cell Signaling Technology, cat# 9661, 1:200) and 4-HNE (Abcam cat# ab46545, 1:300), IL-6 (R&D systems, cat# MAB206, 100ng/ml), IL-8 (R&D systems, cat#MAB208, 100ng/ml), MCP-1 (R&D systems,cat#AB279, 100ug/ml).

Validation

We used commercially available antibodies. We relied on the literature cited and data from manufacturers for validation purposes.
Citations:
1) HIF1 - https://www.bdbiosciences.com/en-eu/products/reagents/microscopy-imaging-reagents/immunofluorescence-reagents/purified-mouse-anti-human-hif-1.610958
2) HK-2 - https://www.cellsignal.com/products/primary-antibodies/hexokinase-ii-c64g5-rabbit-mab/2867
3) p-STAT3 Tyr 708 - https://www.cellsignal.com/products/primary-antibodies/phospho-stat3-tyr705-antibody/9131
4) total STAT3 - https://www.cellsignal.com/products/primary-antibodies/stat3-124h6-mouse-mab/9139
5) GAPDH - https://www.cellsignal.com/products/primary-antibodies/gapdh-d16h11-xp-rabbit-mab/5174
6) β-Actin - https://www.sigmaaldrich.com/US/en/product/sigma/a5441
7) GPAT3 - https://www.novusbio.com/products/agpat9-antibody_nbp1-93692#datasheet
8) Ki-67 - https://tools.thermofisher.com/content/sfs/brochures/D12536~.pdf
9) cleaved caspase 3 - https://www.cellsignal.com/products/primary-antibodies/cleaved-caspase-3-asp175-antibody/9661?_=1686164268435&Ntt=9661&tahead=true
10) 4-HNE - https://www.abcam.com/products/primary-antibodies/4-hydroxynonenal-antibody-ab46544.html
11) IL-6 - https://www.rndsystems.com/products/human-primate-il-6-antibody-6708_mab206#product-citations
12) IL-8 - https://www.rndsystems.com/products/human-il-8-cxcl8-antibody-6217_mab208#product-citations
13) MCP-1 - https://www.rndsystems.com/products/human-ccl2-je-mcp-1-antibody_ab-279-na#product-citations

Eukaryotic cell lines

Policy information about cell lines and Sex and Gender in Research

Cell line source(s)

SKOV3ip1: Gordon Mills, University of Texas MD Anderson Cancer Center, Houston
OVCAR5: Gordon Mills, University of Texas MD Anderson Cancer Center, Houston
HeyA8: Gordon Mills, University of Texas MD Anderson Cancer Center, Houston
TYKnu: Gottfried Koneczny, University of California, Los Angeles
293T: Lucy Godley, Northwestern University, Chicago, IL - original source, ATCC

Authentication

All cell lines were routinely authenticated by short tandem repeat profiling using services of IDEXX laboratory Inc. Testing was carried out every three months.

Mycoplasma contamination

All cell lines were routinely tested for mycoplasma contamination using services of IDEXX laboratory Inc and cell lines negative for mycoplasma was used for experiments.

Commonly misidentified lines
(See ICLAC register)

No commonly misidentified lines were used.

Animals and other research organisms

Policy information about studies involving animals; ARRIVE guidelines recommended for reporting animal research, and Sex and Gender in Research

Laboratory animals

We used female six week old athymic nude mice (Harlan Envigo) for xenograft studies.

Wild animals	No wild animals were used.
Reporting on sex	Since we studied ovarian cancer, only female mice were used.
Field-collected samples	The study did not involve samples from the field.
Ethics oversight	All animal studies were approved by the Institutional Animal Care and Use Committee at the University of Chicago.

Note that full information on the approval of the study protocol must also be provided in the manuscript.